MET O 11 TECHNICAL NOTE No. 122

An investigation of various subgridscale condensation schemes

by

R. W. RIDDAWAY

Abstract

Various subgridscale condensation schemes are investigated and their characteristics examined. Incorporation of some of the schemes into the 10-level model resulted in beneficial effects on both the intensity and distribution of the rainfall; the dynamic rain was increased and the convective rain decreased but overall there was a net increase in rainfall. Subgridscale condensation schemes also provide useful information about cloud cover.

Meteorological Office (M.O.11
London Road
Bracknell
Berkshire
United Kingdom

1. Introduction

Most numerical weather prediction models only allow condensation to occur when a grid box is completely saturated; any condensed water then falls out as rain. This approach ignores the existence of cloud and the possibility that only a part of a grid box is cloudy. To overcome these deficiencies subgridscale condensation schemes have been proposed by Jonas (1976), Manton and Cotton (1977), and Sommeria and Deardorff (1977); hereafter these will be referred to as J, M-C and S-D, respectively. All of these schemes have the property that cloud forms before a grid box is completely saturated.

Subgridscale condensation schemes are all based on the same basic assumption that after condensation occurs the amount of cloud liquid water in a grid box is a function of the total water mixing ratio and the saturation mixing ratio only. The different subgridscale condensation schemes are characterised by the assumptions that are made in order to derive this function.

The J scheme is the only one that has been tested in a numerical weather prediction model. It was found that the main benefits were to sharpen the rain belts and to produce a significant increase in rainfall during the first 6 hours so that the accumulated rain in this period became similar to that during any subsequent period. The disadvantages of using this, or any such scheme, are that it requires about 10% more computing time and that it is necessary to store the cloud liquid water as a model variable.

In this report we consider the differences between various subgridscale condensation schemes and suggest a way of estimating appropriate standard deviations. A method of initialising the cloud liquid water will be described and a simple interpretation of subgridscale condensation schemes will be discussed. Finally the beneficial effects of using these schemes will be investigated and cloud forecasts will be examined.

2. The basic equations

Let $\bar{\theta}_0$, $\bar{r}_0$ and $\bar{c}_0$ be the mean values of potential temperature, humidity mixing ratio and cloud liquid water mixing ratio in a grid box before

condensation occurs, and let $\bar{\theta}_i$, $\bar{r}_i$ and $\bar{c}_i$ be the corresponding values after condensation. Since heat and moisture are conserved we have

$$\pi(\bar{\theta}_i - \bar{\theta}_0) = -\frac{L}{c_p}(\bar{r}_i - \bar{r}_0) \tag{2.1}$$

$$\bar{w}_i = \bar{r}_i + \bar{c}_i = \bar{r}_0 + \bar{c}_0 = \bar{w}_0 \tag{2.2}$$

where $\pi = \left(\frac{p}{1000}\right)^{0.286}$ and $\bar{w}$ is the total water mixing ratio. Combining (2.1) and (2.2) gives

$$\bar{\theta}_i - \frac{L}{c_p}\frac{1}{\pi}\bar{c}_i = \bar{\theta}_0 - \frac{L}{c_p}\frac{1}{\pi}\bar{c}_0 \tag{2.3}$$

The liquid water potential temperature $\bar{\theta}_L$ is defined as $\bar{\theta}_L = \bar{\theta} - \frac{L}{c_p}\frac{1}{\pi}\bar{c}$ and so (2.2) and (2.3) show that both $\bar{w}$ and $\bar{\theta}_L$ are conserved during condensation.

We now make the basic assumption that after condensation the amount of liquid water is only a function of the total water and saturation mixing ratios (this function will be denoted by $\hat{c}$). Therefore the cloud liquid water mixing ratio after condensation is given by

$$\bar{c}_i = \hat{c}[\bar{w}_i, \bar{r}_{si}] \quad \text{with} \quad \bar{r}_{si} = r_s[\bar{T}_i] \tag{2.4}$$

Substituting (2.4) in (2.3) and rearranging gives

$$\pi(\bar{\theta}_i - \bar{\theta}_0) = \frac{L}{c_p}\left(\hat{c}[\bar{w}_i, \bar{r}_{si}] - \bar{c}_0\right) \tag{2.5}$$

Expanding $\hat{c}$ about the state before condensation yields

$$\hat{c}[\bar{w}_i, \bar{r}_{si}] = \hat{c}[\bar{w}_0, \bar{r}_{si}]$$

$$\approx \hat{c}[\bar{w}_0, \bar{r}_{s0}] + \left.\frac{\partial \hat{c}}{\partial \bar{r}_s}\right|_0 (\bar{r}_{si} - \bar{r}_{s0}) \tag{2.6}$$

The Clausius-Clapeyron equation is used to relate changes in saturation mixing ratio to changes in temperature, so

$$\bar{r}_{si} - \bar{r}_{s0} \approx \chi[\bar{T}_0]\pi(\bar{\theta}_i - \bar{\theta}_0) \tag{2.7}$$

with

$$\chi[\bar{T}_0] = \frac{\varepsilon L}{R}\frac{r_s[\bar{T}_0]}{\bar{T}_0^2}$$

If $\beta = -\left.\frac{\partial \hat{c}}{\partial \bar{r}_0}\right|_0$, then substituting (2.6) and (2.7) in (2.5) and rearranging gives

$$\pi(\bar{\theta}_i - \bar{\theta}_0) = \frac{L}{c_p}\frac{\left(\hat{c}[\bar{w}_0, \bar{r}_{s0}] - \bar{c}_0\right)}{\left(1 + \frac{L}{c_p}\chi[\bar{T}_0]\beta\right)} \qquad (2.8)$$

If A_0 is defined such that $\pi(\bar{\theta}_i - \bar{\theta}_0) = \frac{L}{c_p}A_0$, then the values of $\bar{\theta}$, $\bar{r}$ and $\bar{c}$ after condensation are

$$\begin{aligned} \bar{\theta}_i &= \bar{\theta}_0 + \frac{L}{c_p}\frac{A_0}{\pi} \\ \bar{r}_i &= \bar{r}_0 - A_0 \\ \bar{c}_i &= \bar{c}_0 + A_0 \end{aligned} \qquad (2.9)$$

These equations were used by J, S-D and M-C in their subgridscale condensation schemes, but they made different assumptions in deriving $\hat{c}$. It is worth noting that if all the water in excess of $\bar{r}_{s0}$ is condensed out we have $\hat{c}[\bar{w}_0, \bar{r}_{s0}] = \bar{w}_0 - \bar{r}_{s0}$ and $\beta = 1$, and so (2.8) reduces to

$$\pi(\bar{\theta}_i - \bar{\theta}_0) = \frac{L}{c_p}\frac{(\bar{r}_0 - \bar{r}_{s0})}{\left(1 + \frac{L}{c_p}\chi[\bar{T}_0]\right)}$$

which is identical to the expression used by Burridge and Gadd (1977) in the 10-level model.

3. The derivation of $\hat{c}$ and β

J assumed that after condensation has occurred the total water relative humidity $H = w/r_s$ in a grid box is distributed normally about a mean value $\bar{H}$ with a standard deviation σ_H. Hence the fraction of the grid box in which the total relative humidity lies between H and $H+dH$ is

$$f(H)\,dH = \frac{1}{\sqrt{2\pi}\,\sigma_H}\exp\left[\frac{-(H-\bar{H})^2}{2\sigma_H^2}\right]dH \qquad (3.1)$$

The fraction of the grid box containing cloud is

$$\alpha = \int_1^\infty f(H)\,dH \qquad (3.2)$$

and the cloud liquid water mixing ratio $\hat{c}$ is given by

$$\frac{\hat{c}}{\bar{r}_s} = \int_1^\infty (H-1)\, f(H)\, dH \qquad (3.3)$$

Using (3.1) in (3.2) and (3.3) gives

$$\alpha = \frac{1}{2}\left(1 + \mathrm{erf}\left[\frac{Q}{\sqrt{2}}\right]\right) = E(Q)$$

$$\frac{\hat{c}}{\bar{r}_s \sigma_H} = \alpha Q + \frac{1}{\sqrt{2\pi}} \exp\left[-\frac{Q^2}{2}\right] = F(Q) \qquad (3.4)$$

$$Q = \frac{\bar{H}-1}{\sigma_H}$$

where erf is the error function.

S-D argued that, since the total water (w) and the liquid water potential temperature $\left(\theta_L = \theta - \frac{L}{c_p}\frac{c}{\pi}\right)$ are both conserved during condensation, it is these quantities that should have a joint normal probability function (G say), so that

$$\alpha = \int_{-\infty}^{\infty}\int_{r_s}^{\infty} G\, dw\, d\theta_L$$

$$\hat{c} = \int_{-\infty}^{\infty}\int_{r_s}^{\infty} (w - r_s)\, G\, dw\, d\theta_L$$

S-D had to make several approximations in order to integrate these equations, but later Mellor (1977) showed that these were self-cancelling.

If the fractional variations in θ_L are small compared with those in w we can derive expressions for α and $\hat{c}$ which are analagous to (3.4). In doing this it is convenient to introduce the notation

$$r_{sL} = r_s[T_L] \quad \text{and} \quad T_L = T - \frac{L}{c_p} c$$

We then have

$$\alpha = E(Q) \qquad \frac{\hat{c}}{\lambda b \bar{r}_s \sigma_{HL}} = F(Q) \qquad Q = \frac{\bar{H}-b}{b\sigma_{HL}} \qquad (3.5)$$

with $\bar{r}_{sL} = r_s[\bar{T}_L] = b\bar{r}_s \qquad \chi_L = \frac{\varepsilon L}{R}\frac{\bar{r}_{sL}}{\bar{T}_L^2} \qquad \bar{T}_L = \bar{T} - \frac{L}{c_p}\bar{c}$

$$\lambda = \frac{1}{\left(1 + \frac{L}{c_p}\chi_L\right)} \quad \text{and} \quad b = \frac{1}{\left(1 + \frac{L}{c_p}\chi_L \frac{\bar{c}}{\bar{r}_{sL}}\right)}$$

Here σ_{HL} is the standard deviation of $H_L = w/r_{sL}$ and the functions E and F are defined in (3.4).

M-C assumed that the total water and potential temperature (w and θ) have a joint normal probability function. If this is used and the previous analysis repeated, we find that α, $\hat{c}$ and Q are given by (3.5) with σ_{HL} replaced by σ_H and $\lambda = L = 1$ $(\chi_L = 0)$. The equations are then identical to those used by J (see (3.4)). Therefore, provided the fractional variations in are much smaller than those in w, the schemes devised by J and M-C are the same.

Now consider whether there is any significant difference between the formulations of J and S-D given by (3.4) and (3.6). For comparison purposes we use the ICAO values of temperature and assume that $\bar{c}/\bar{r}_s = 10\%$. Therefore λ and L may be depicted as functions of pressure only (see Figure 1). Throughout the troposphere L is close to 1 and this is also true when other values of $\bar{T}$ and $\bar{c}$ are used. Therefore as a first approximation L has a value of 1. The value of λ depends only weakly upon $\bar{c}$, but does vary with temperature, and in general λ will always be significantly different from 1 in the lower troposphere. This means that the main difference between the schemes of J and S-D lies in the value of λ The results of using both these schemes will be discussed later.

Following S-D it is convenient to have approximate expressions for E(Q) and F(Q) which preserve the basic relationship

$$\frac{\partial F}{\partial Q} = E \qquad (3.6)$$

Therefore we use

	E(Q)	F(Q)	
$Q \leq -1.6$	0	0	
$-1.6 < Q \leq 1.6$	$(Q+1.6)/3.2$	$(Q+1.6)^2/6.4$	(3.7)
$1.6 < Q$	1	Q	

Now consider the derivation of $\beta = -\frac{\partial \hat{c}}{\partial \bar{r}_s}$ for the S-D method (the value of β for the J method follows by setting $\lambda = L = 1$). If (3.5) is differentiated with respect to $\bar{r}_s$ and the derivatives of λ, L and σ_{HL} neglected then

$$\beta = -\frac{\partial \hat{c}}{\partial \bar{r}_s} = -\lambda L \sigma_{HL} \left(F[Q] + \bar{r}_s \frac{\partial F[Q]}{\partial \bar{r}_s} \right)$$

But

$$\frac{\partial F}{\partial \bar{r}_s} = \frac{\partial F}{\partial Q}\frac{\partial Q}{\partial \bar{r}_s} = \frac{-\alpha \bar{H}}{L \bar{r}_s \sigma_{HL}}$$

and so β becomes

$$\beta = \alpha\lambda\bar{H} - \frac{\hat{c}}{\bar{r}_s} \qquad (3.8)$$

The general procedure at each time step for including subgridscale condensation in numerical models is as follows.

(i) Advect the model variables to give $\bar{\theta}_0$, $\bar{r}_0$ and $\bar{c}_0$; if we do not wish to advect cloud liquid water then $\bar{c}_0$ is the same as the value at the previous time step.

(ii) Compute $\bar{T}_L$, L and λ using $\bar{c}_0$ and $\bar{r}_{s0}$

(iii) Calculate $\bar{H} = \bar{w}_0/\bar{r}_{s0}$ and use (3.5) to find Q, α and $\hat{c}$

(iv) Compute β from (3.8) and then evaluate the model variables after condensation ($\bar{\theta}_i$, $\bar{r}_i$ and $\bar{c}_i$) using (2.9).

(v) Calculate how much cloud liquid water is converted into rainwater (this is discussed in Section 7).

In order to use this procedure it is necessary to diagnose the cloud liquid water at the start of a forecast.

4. The initial values of cloud liquid water

One convenient way of deriving initial values of cloud liquid water is to assume that the analysed fields of relative humidity and temperature are representative of the atmosphere after condensation has taken place - but before any of the cloud has been converted to rain. Therefore the cloud liquid water mixing ratio is given by $\hat{c}$.

We use the S-D formulation (see (3.5)) with $\bar{c}$ replaced by $\hat{c}$ in the computation of L, λ and $\bar{H}$, and introduce the relative humidity of water vapour and cloud liquid water ($\tilde{H}$ and H^*) given by

$$\tilde{H} = \frac{\bar{r}}{\bar{r}_s} \qquad H^* = \frac{\hat{c}}{\bar{r}_s} \quad \text{with} \quad \bar{H} = \frac{\bar{w}}{\bar{r}_s} = \tilde{H} + H^*$$

If $(1 - 1.6\sigma_{HL}) \leq \bar{H}/t \leq (1 + 1.6\sigma_{HL})$ then we use the approximate expression for F(Q) (see (3.7)) to give

$$H^* = \lambda t \sigma_{HL} F(Q) = \frac{\lambda t \sigma_{HL}}{6.4} \left(\frac{\bar{H} - t + 1.6\sigma_{HL}}{t\sigma_{HL}} \right)^2 \qquad (4.1)$$

where λ, t and σ_{HL} were defined in the previous section. Since $1/\bar{T}_L^2 \approx 1/\bar{T}^2$ we have

$$\frac{\chi[\bar{T}_L]}{r_s[\bar{T}_L]} \approx \frac{\chi[\bar{T}]}{r_s[\bar{T}]} = \frac{c_p}{L} \frac{\bar{X}}{r_s[\bar{T}]} \quad \text{say}$$

and so $$t = \frac{1}{1 + \bar{X} H^*} \quad \text{and} \quad \lambda = \frac{1 + \bar{X} H^*}{1 + \bar{X}(H^* + 1)} \qquad (4.2)$$

Substituting (4.2) in (4.1) and assuming $\tilde{H} \gg H^*$ we have a cloud liquid water relative humidity of

$$H^* = \frac{(\tilde{H} - \tilde{H}_c)^2}{6.4\sigma_{HL}(1+\bar{X}) - 2(\tilde{H} - \tilde{H}_c)(1 + \bar{X}\tilde{H} + 1.6\sigma_{HL}\bar{X})} \qquad (4.3)$$

where $\tilde{H}_c = 1 - 1.6\sigma_{HL}$ is the value of relative humidity below which there is no cloud. Also when $H^* \ll 1$ we have $t \approx 1$ and $\lambda \approx 1/(1+\bar{X})$, and so in the lower troposphere where $\bar{X} \approx 1$ we have $\lambda \approx 0.5$ which is consistent with the results given in Figure 1.

Although (4.3) is in terms of the vapour relative humidity $\tilde{H}$, the range of humidities for which it is valid is still given in terms of the total relative humidity $\bar{H}$. However it can be shown that if $\bar{H}/t = (1 + 1.6\sigma_{HL})$ we have $\tilde{H} = 1$; also when $\bar{H}/t = (1 - 1.6\sigma_{HL})$ we have $t = 1$ which gives $\tilde{H} = (1 - 1.6\sigma_{HL}) = \tilde{H}_c$. Therefore the cloud liquid water can be initialised by setting $H^* = 0$ when $\tilde{H} < \tilde{H}_c$ and using (4.3) when $\tilde{H}_c \leq \tilde{H} \leq 1$ We then compute $\hat{C}$ from $\hat{C} = H^* F_s$.

This procedure could be used to provide initial values of the cloud liquid water relative humidity H^* or alternatively as just a first guess in an interative scheme to find H^*. In the following experiments an iterative procedure is used.

When the J method is used the equivalent expression to (4.3) is found by setting $\lambda = L = 1$ (ie use $\bar{X} = 0$) and replacing σ_{HL} by σ_H .

5. An interpretation of the condensation schemes

The condensation schemes derived in Sections 2 and 3 can be interpreted in a simple way. First consider the J scheme. We again use the cloud liquid water relative humidity $H^* = \hat{c} / \bar{r}_s$, so (3.4) becomes

$$\frac{H^*}{\sigma_H} = F(Q)$$

Using (3.6), this gives $\frac{\partial}{\partial Q}\left(\frac{H^*}{\sigma_H}\right) = \alpha$

But since $\frac{\partial}{\partial Q} = \sigma_H \frac{\partial}{\partial \bar{H}}$ we now have $\frac{\partial H^*}{\partial \bar{H}} = \alpha$

If $\delta H^*, \delta \tilde{H}$ and $\delta \bar{H}$ are increments in the relative humidities of the cloud liquid water, water vapour and total water, then

$$\delta H^* = \alpha \, \delta \bar{H} \quad \text{and} \quad \delta \tilde{H} = (1-\alpha) \, \delta \bar{H} \qquad (5.1)$$

Hence any change in the total water relative humidity is distributed between the cloud liquid water and water vapour relative humidities according to the fractional cloud volume α . Louis (1977) has used this as a basic assumption in his scheme to parameterise the vertical eddy fluxes due to convection in terms of a diffusion formula.

Now consider the S-D scheme. It is convenient to introduce relative humidities with respect to $\bar{r}_{sL} = r_s[\bar{T}_L]$ instead of $\bar{r}_s$. Define $H_L^*, \tilde{H}_L$ and $\bar{H}_L$ by

$$H_L^* = \frac{\hat{c}}{\bar{r}_{sL}} \qquad \tilde{H}_L = \frac{\bar{r}}{\bar{r}_{sL}} \qquad \bar{H}_L = \frac{\bar{w}}{\bar{r}_{sL}}$$

Since λ is almost constant for a given value of σ_{HL} , we find that the above procedure gives

$$\delta H_L^* \simeq \alpha \lambda \, \delta \bar{H}_L \quad \text{and} \quad \delta \tilde{H}_L = (1 - \alpha\lambda) \, \delta \bar{H}_L \qquad (5.2)$$

Hence any change in $\bar{H}_L$ is distributed according to $\alpha\lambda$. To a good approximation we can replace $\bar{F}_{SL}$ by $\bar{F}_S$, so (5.2) may be written as

$$\delta H^* \approx \alpha\lambda\, \delta\bar{H} \quad \text{and} \quad \delta\tilde{H} = (1-\alpha\lambda)\,\delta\bar{H} \qquad (5.3)$$

In the S-D scheme $\lambda < 1$ and so, for a given α , a smaller proportion of $\delta\bar{H}$ goes into cloud water than for the J scheme. Therefore, for a given total water relative humidity $\bar{H}$, the cloud liquid water derived from the S-D scheme is always less than that from the J scheme.

6. Estimates of σ_H and σ_{HL}

Ricketts (1973) investigated the relationship between cloud cover and relative humidity. There was a large amount of scatter in the results but the fractional cloud cover did tend to increase with increasing relative humidity. The essential features of Ricketts results have been used in the 10-level model to relate the fractional cloud cover (f say) for high, medium and low cloud to the relative humidity of the moistest 100 mb layer in the 300-500 mb, 500-800 mb and 800-1000 mb groups respectively (see Burridge and Gadd (1977)); the relationships are shown in Figure 2a.

We now use estimates of the cut-off relative humidity below which there is no cloud ($\tilde{H}_c$ say) to compute the standard deviations required for the condensation schemes. From Figure 2a $\tilde{H}_c$ is estimated for several 100 mb layers

Cloud type	layer (mb)	$\tilde{H}_c$	σ	P(mb)
high	400-500	0.35	0.41	450
medium	-	0.44	0.35	-
low	800-900	0.54	0.29	850

For both subgridscale condensation schemes described in Section 3 α becomes zero when Q = -1.6 (see (3.4), (3.5) and (3.7)). Therefore

$$\sigma = \frac{(1-\tilde{H}_c)}{1.6} \qquad (6.1)$$

where σ is an estimate of the standard deviation of $H = W/\Gamma_S$ or $H_L = W/\Gamma_{SL}$ depending upon if we use the J or S-D scheme. The values of σ derived in this way are given above. The increase in σ with altitude may be interpreted as meaning that low level layered clouds tend to cover large regions both horizontally and vertically so that there is relatively little variation in humidity in a given volume. Higher up the clouds tend to be more limited in extent which results in a greater variability in the humidity. However since radio-sondes tend to underestimate high level humidities the derived σ at 450 mb may well be an over-estimate. Assuming a linear variation of σ with p we have

$$\sigma(p) = 0.29 + 0.12\,\frac{(850 - p)}{400} \qquad (6.2)$$

J examined some ascents and concluded that σ should be treated as a function of the water vapour relative humidity $\tilde{H}$; he then chose

$$\sigma(\tilde{H}) = 0.2\,(2 - \tilde{H}) \qquad (6.3)$$

Using this in (6.1) gives a cut-off relative humidity of $\tilde{H}_c = 0.53$ at all levels.

Subgridscale condensation schemes give the fractional cloud volume α_i in a layer i . Therefore in order to compute a cloud cover we must combine the cloud volumes from adjacent layers. A reasonable estimate of the fractional cloud cover f for n layers is

$$f = 1 - \prod_{i=1}^{n} (1 - \alpha_i) \qquad (6.4)$$

For comparison purposes we use this to estimate f for low cloud by assuming that the relative humidity is the same in the 1000-900 mb and 900-800 mb layers. A similar procedure is followed to compute f for medium and high cloud with the groups of layers used by Burridge and Gadd.

Figures 2b and 2c show the results of using the S-D method with (6.2) and the J method with (6.3). Both of these reproduce the main features of Figure 2a. However it is difficult to interpret the differences because, in subgridscale condensation schemes, rain forms before the vapour relative humidity $\tilde{H}$ reaches 100% and thus will limit the likely range of $\tilde{H}$.

7. The conversion of cloud into rain

Once we have computed the amount of cloud liquid water that is present after condensation ($\bar{c}_i$) it is necessary to consider how much of the cloud water is converted into rain. If $\bar{P}$ is the grid-mean value of the conversion rate and Δt the time step, then the amount of cloud liquid water and rain water after conversion ($\bar{c}_f$ and $\bar{m}_f$ say) is

$$\bar{c}_f = \bar{c}_i - \bar{P}\,\Delta t$$
$$\bar{m}_f = \bar{P}\,\Delta t$$

Kessler (1969) suggested that the conversion rate could be split into two parts; autoconversion which results from the relative motion between cloud drops and collection which is caused by raindrops coalescing with cloud drops. Let $P_a(c)$ and $P_c(c,m)$ be the autoconversion and collection rates within a cloud with cloud liquid and rain water contents of c and m . The total conversion rate is then

$$P = P_a(c) + P_c(c,m)$$

and its grid-mean value is

$$\bar{P} = \alpha P_a\left(\frac{\bar{c}}{\alpha}\right) + \alpha P_c\left(\frac{\bar{c}}{\alpha}, \frac{\bar{m}}{\alpha}\right) = \bar{P}_a + \bar{P}_c \qquad (7.1)$$

where $\bar{c}$ and $\bar{m}$ are the grid-mean values of cloud liquid water and rain water, and α is the fractional cloud volume.

In Appendix I we discuss the choice of expressions for P_a and P_c .

In the following study we use

$$P_a = \frac{\alpha}{\tau_a}\left(c - \frac{l\,\tau_s}{\alpha}\right) \qquad (7.2)$$

with $l = 0.07$ and $\tau_a = 10^3$ sec. This is a modification of the expression used by J where we have tried to allow for the following behaviour

(i) autoconversion is likely to be easier in large clouds than small ones.

(ii) the autoconversion time constant tends to increase with increasing vertical velocity.

In Appendix II we present some results which support the use of $l = 0.07$ in (7.2).

The collection rate is based on the expression derived by Kessler, but allowance has been made for the fact that thick clouds tend to produce more rain than thin ones; we use

$$P_c = \frac{\alpha}{\tau_c} c M F^{1/2} \qquad (7.3)$$

where $F = (\rho/\rho_0)$, $\rho_0 = 1.2\ kg\ m^{-3}$ and $\tau_c = 310$ sec.

The use of (7.1) and (7.3) is simplified if we assume that only rain formed in a given layer takes part in the collection process. This leads to a purely local collection rate of

$$P_c = \alpha \frac{c}{\tau_c} \left(\frac{\Delta p\, P_a}{\omega_t} \right) F^{1/2} \qquad (7.4)$$

where $\omega_t = 0.6 F^{1/2}\ mb\ s^{-1}$ is the fall speed of raindrops and Δp is the pressure thickness of the layer. Using (7.4) in (7.1) with $\Delta p = 100\ mb$ gives

$$\bar{P} = \bar{P}_a (1 + 0.538\, \bar{c}\, F^{-1/2}) \qquad (7.5)$$

where $\bar{P}_a$ is derived from (7.2).

J suggested a single expression for the total conversion rate $\bar{P}$; he used

$$\bar{P} = \frac{1}{\tau} (\bar{c} - 0.15 \alpha \bar{\Gamma}_s) \qquad \tau = 720\ s \qquad (7.6)$$

and this will also be used in some of the following experiments.

8. The properties of different schemes

One of the basic features of all the schemes described is that rain is allowed to form before the mean relative humidity over the grid box reaches 100%. The critical relative humidity at which rain forms ($\tilde{H}_R$ say) depends upon several factors:

(i) whether $H = W/\Gamma_s$ or $H_L = W/\Gamma_{SL}$ is assumed to have a normal distribution ((3.4) or (3.5)); these two options will be denoted by S and J.

(ii) the assumed form of the standard deviation ((6.2) or (6.3)); these will be denoted by R and J.

(iii) the assumed rate of conversion of cloud into rain ((7.5) or (7.6)); these will be denoted by R and J.

Different combinations of these will be labelled (i)/(ii)/(iii).

Figure 3 shows the variation of $\tilde{H}_R$ with pressure for several different schemes, including the present operational scheme denoted by O_ρ . Perhaps the most striking feature of these results is that the choice of method (compare S/J/J with J/J/J), standard deviation (compare S/R/R with S/J/R) and conversion rate (compare S/R/J with S/R/R) can have a marked effect on the behaviour of

Both J/J/J and J/J/R give a constant $\tilde{H}_R$ that is, in the lowest levels, much less than that for the other schemes. This may produce problems in the lower levels because over the sea the air is often very moist with humidities in excess of 80% although no rain is actually falling. Hence we may get spurious rain near anticyclones. The behaviour of S/R/J, S/R/R and S/J/R is similar in the lower levels although markedly different higher up. The S/J/J combination appears to be little improvement on the operational scheme.

Although Figure 3 is useful in that it illustrates the differences between various schemes, the results can be misleading. For example in some cases a subgrid-scale condensation scheme can be harmful in the sense that it takes longer for rain to form than in the present operational scheme. This can be illustrated by considering the S-D scheme. If the total water relative humidity changes by $\delta\bar{H}$ then (5.3) shows that there is an associated change in vapour relative humidity such that

$$\delta\bar{H} = \frac{1}{(1-\alpha\lambda)}\delta\tilde{H} = \phi\,\delta\tilde{H} \quad \text{say} \qquad (8.1)$$

Here α is the fractional cloud volume and $\lambda = \lambda[\bar{T}_L, p]$ - see Section 3. For the J scheme (8.1) still holds if we set $\lambda = 1$. If $\tilde{H}_R$ is the vapour relative humidity at which rain forms then the area beneath a plot of ϕ against $\tilde{H}$ between a given starting relative humidity $\tilde{H}_0$ and $\tilde{H}_R$ is an indication of how much moisture must be made available before rain forms. Figure 4 shows such a plot for 850 mb for several schemes. Calculation of the integral of (8.1) shows that for all $\tilde{H}_0$ both J/J/J and S/R/R require less moisture to reach their appropriate $\tilde{H}_R$ than does the operational scheme. Also we find that for $\tilde{H}_0 < 80\%$ both subgridscale condensation schemes require similar amounts of moisture to reach

$\tilde{H}_R$ whereas when $\tilde{H}_0 > 80\%$ J/J/J requires slightly less moisture than S/R/R; at higher levels S/R/R usually needs less moisture than J/J/J. These results suggest that overall the performance of the two condensation schemes should be similar.

We now consider the S/J/J scheme. Figure 3 gives the impression that at lower levels this scheme is similar to the operational scheme. However the results in Figure 4 clearly show that for all $\tilde{H}_0$ the S/J/J requires more moisture to reach $\tilde{H}_R$ than does the operational version. These results illustrate that the incorporation of a subgridscale condensation scheme into a numerical model will not necessarily allow the "early" formation of rain.

9. The initial rainfall fields

We now examine in detail the initial rainfall fields for one particular case (00Z 30/6/77). However many of the following comments are generally applicable.

Unfortunately there is very little information about the actual rate and distribution of rainfall in the rectangle area due to the sparse data coverage. However the surface observations, along with their analysis, allows us to distinguish likely areas of rainfall and to some extent the intensity. Figure 5 shows the surface analysis and the observations of cloud and present weather where there is either rainfall or 6/8 th or more of cloud. There appears to be three main areas of precipitation.

(i) There is a complex rain area in the Central Atlantic with the heaviest rain likely to be near the triple point. There is drizzle in the warm sector and rain associated with the northern portion of the cold front. On the southern portion there is a wave which has phased in with a trough in the cold air; there is continuous rain in the trough and there is likely to be rain associated with the wave. Thereis some rain near Cape Farewell.

(ii) There is rain in the vicinity of the low to the south of Iceland and its associated fronts; the heaviest rain is near Iceland and Ireland.

(iii) There is rain near the low over Sweden. There is an associated occlusion, but the southern portion is not very active although there is rain in a nearby trough situated over southern Germany.

Since the humidity analyses depend upon the background field it is instructive to examine the 12 hour forecast valid at 00Z 30/6/77 (see Figure 6). Comparison of the actual and forecast charts, Figures 5 and 6, shows that the forecast reproduced all the main rain areas. However there is one important error in the forecast; the European rain belt has been forecast to extend into the Bay of Biscay and Northern Spain. Therefore it is likely that the analysed humidities at 00Z 30/6/77 will be too high in this region.

We now examine the initialised rainfall derived from the J/J/J and S/R/R schemes. Figures 7a and 7b show the initialised rate of dynamic rain using J/J/J. Most of the rain area described earlier are apparent, but the rainfall tends to be too extensive and in some places too heavy. Some of the significant features are:

(i) the erroneous widespread rain to the south-east of Newfoundland due to a combination of moist lower layers and a high low rainfall humidity threshold (see Figure 3).

(ii) no rain in the warm sector over much of the British Isles due to the low analysed relative humidities.

(iii) the rain belt near the British Isles extends southwards into the Bay of Biscay due to the erroneously high analysed relative humidities; the rainfall rate is also rather excessive.

Figures 7c and 7d show the results using S/R/R. The rainfall near the British Isles and over the continent is quite reasonable except for the rain in the Bay of Biscay whose origin has already been discussed. In the Central Atlantic the main rain area has been reproduced quite well and there is some dynamic rain associated with the trailing cold front. There is also a considerable improvement over J/J/J in the southwest corner of the chart.

Overall the initialised rainfall using S/R/R is superior to that using J/J/J; this was also true in other cases that were examined. However it should be noted that this is not really a fair test of either scheme because we should use humidity analyses which are based on background fields derived from forecasts using the appropriate condensation scheme.

10. Forecast rainfall fields

J has described a series of forecasts which use J/J/J and found that there was "an overall increase of between 5% and 10% in the rainfall accumulations and that

the rainfall in the initial stages of the forecast is comparable with that at later stages". These conclusions are supported by experiments conducted in this study and so we will concentrate upon the differences between J/J/J and S/R/R; forecasts based on 00Z 30/6/77 will be used to illustrate these. We, first consider a 6 hour forecast.

Figure 8 shows the operational forecast. By T+6 large areas of dynamic rain have evolved (see Figure 8b) and these are consistent with the distribution of accumulated dynamic rain (see Figure 8d). This consistency is a desirable property of any condensation scheme. Comparisons of Figures 8c and 8d shows that during the first 6 hours there is a preponderance of convective rain (this will be considered further later).

Figures 9 and 10 show the results for S/R/R and J/J/J. At T+6 both have similar distributions of rain although the rain to the southeast of Newfoundland is rather incoherent for J/J/J. Figures 11b and 11d illustrate that the J/J/J initial fields are not very consistent with those in the subsequent forecast; in this respect S/R/R is superior as indicated by Figures 10b and 10d. Comparisons between the subgridscale condensation schemes and the operational version show that the new schemes tend to produce less convective rain (eg in Central Atlantic) and more coherent rain belts (eg over the continent and UK).

It is instructive to consider the rainfall in more detail with the aid of Figure 11 which shows 6 hourly mean rainfall accumulations. During the first 6 hours all three schemes produce similar amounts of rain although in other cases studied, the subgridscale condensation schemes produced increases up to 20%. However there are marked differences in the proportion of convective and dynamic rain. For the operational version the proportion of rain of dynamic origin in the first period is 17% compared with an average of 59% during the following periods; the corresponding figures for S/R/R are 66% and 85% (results for J/J/J are similar). Therefore the new condensation schemes make the rainfall characteristics during the first 6 hours more like those of succeeding periods. Also the overall effect of these schemes is to increase the dynamic rain, decrease the convective rain and produce a net increase in rainfall (in this case by about 9%); there is some evidence that all these are desirable.

The 36 hour forecast using the operational version is shown in Figure 12 and the corresponding results for S/R/R are given in Figure 13 (S/R/R and J/J/J yield similar results). The main effects of using S/R/R in place of the operational version are to augment the dynamic rain in the rain belt near Nova Scotia and to increase the structure of the rainfall in mid-Atlantic. Also the coverage of convective rain has been reduced and the grid-point storms eliminated. It is difficult to evaluate these differences but comparison with the verifying analysis (Figure 14) indicates that the use of a subgridscale condensation scheme is likely to lead to an improvement in both the distribution and intensity of rainfall.

In the next Section we consider the structure that is apparent in the mid-Atlantic rain belts.

11. The structure of the cloud and rain fields

The surface analysis at 12Z 1/7/77 (Figure 14) and the nephanalysis at about the same time (Figure 15) indicate that in the mid-Atlantic there are two major cloud bands (observations show that these are also rain bands) - one band is of frontal origin and the other associated with a trough. Examination of the forecasts shown in Figures 12 and 13 reveals that the one which used S/R/R reproduced the right kind of structure in the rain fields whereas the one with the operational version of the condensation scheme did not. However in both forecasts there was evidence of a double structure in the relative humidity fields.

Since the existence of cloud is in integral part of the subgridscale condensation scheme we can examine the forecast total cloud cover (f_{tot} say). This is computed from the fractional cloud volume for each layer by using (6.4). The field of f_{tot} at T+36 for S/R/R is shown in Figure 16 (the corresponding rainfall forecasts are in Figure 13). Comparison of Figures 15 and 16 reveals a surprising degree of skill in the forecast. All the main cloudy areas have been reproduced; as well as the frontal cloud note the cloudy areas over Southern Spain and to the east of Greenland. Also there is clearly a double structure in the mid-Atlantic cloud bands and, although not apparent in Figure 16, there is evidence of two separate cloud bands near Nova Scotia.

On Figure 16 are indicated the forecast positions of the main troughs and fronts based on the cloud and rain predictions. Comparison with Figure 14 shows that the forecast features have the right kind of shape and are in roughly the correct position.

The Burridge and Gadd method of deriving cloud cover (see Section 6) gives estimates of high, medium and low cloud. These can also be combined using (6.4) to give f_{tot} and the results of doing this for the 36 hour forecast using the operational condensation scheme are shown in Figure 17. Comparison of this with Figures 15 and 16 indicates that the Burridge and Gadd method overestimates the cloud cover and that overall the results are inferior to the cloud forecasts using the subgridscale condensation scheme.

Concluding remarks

The various experiments described here, along with those performed by J, indicate that the use of a subgridscale condensation scheme usually has a beneficial effect on rainfall forecasts. The benefits are:

(i) an increase in rainfall during the first 6 hours so that the total during this period is similar to that during subsequent periods (this did not happen in the example considered earlier, but it usually does)

(ii) the proportions of dynamic and convective rain during the first 6 hours are similar to those during other periods

(iii) a general increase in total rainfall throughout the forecast

(iv) a marked increase in dynamic rain and decrease in convective rain

(v) an increase in the amount of structure in the rainfall.

Subgridscale condensation schemes also provide information about cloud and we have shown that charts of cloud cover could be useful in the interpretation of forecasts; knowledge of the cloud is also essential for radiation calculations.

In choosing a subgridscale condensation scheme we have to decide upon

(i) the quantities which we assume have a normal probability distribution (or some other kind of distribution)

(ii) the standard deviations (or the corresponding parameters of another kind of basic distribution is used)

(iii) the cloud physics parameterisation.

The choice is important because for some combinations the new scheme may be worse than the operational version.

We have considered in detail two schemes. The first scheme was based on the idea of S-D that the total water and the liquid water potential temperature have joint normal probability distributions. The standard deviation was then derived from the observed dependence of cloud cover upon relative humidity. A relatively sophisticated cloud physics scheme was then chosen; an attempt was made to include the dependence of rain conversion processes on cloud thickness. The second scheme examined was that due to J. The main differences between these two schemes is at the initialisation stage because at low levels the J/J/J has a much lower critical relative humidity for rain formation than does S/R/R; this means that the J/J/J scheme sometimes produces spurious rain in anticyclones.

Overall the results from using J/J/J and S/R/R are similar. This is because both schemes have similar characteristics when we consider how much moisture is required to go from a given initial relative humidity to that at which rain forms. Once rain has formed both schemes convert cloud into rain at a similar rate (although J/J/J gives larger values of cloud liquid water than S/R/R it also has a larger autoconversion threshold).

We conclude that there are many benefits in using a subgridscale condensation scheme and that it is preferable to use S/R/R rather than J/J/J.

Appendix 1

A discussion of the parameterisation of the cloud physics

Here we discuss various formulations that have been used to parameterise the autoconversion and collection processes.

1. Autoconversion

The most widely used expression for the autoconversion rate P_a is that due to Kessler (1969)

$$P_a = \frac{1}{\tau_a}\left(c - \frac{0.5}{\ell}\right) \qquad \text{(A1.1)}$$

However, since our condensation schemes are formulated in terms of humidities, it is convenient to follow Jonas (1976) and introduce an autoconversion threshold that is dependent upon r_s. Jonas chose a threshold such that rain only forms when c/r_s exceeded 0.15. At 850 mb a typical value of r_s is 6 gm/kg, and this gives a threshold cloud liquid water of 0.9 gm/kg, which is almost twice that suggested by Kessler. Therefore, in order that the threshold should be similar to that proposed by Kessler, we use a threshold cloud liquid water relative humidity (ℓ say) of 0.07; we then have

$$P_a = \frac{1}{\tau_a}\left(c - \ell r_s\right)$$

The suitability of using $\ell = 0.07$ is discussed in Appendix 2.

Autoconversion is likely to be easier in large clouds than in small ones due to differences in drop-size spectrum. One way of including this effect is to make the threshold inversely proportional to the cloud amount (as specified by), so that

$$P_a = \frac{1}{\tau_a}\left(c - \frac{\ell r_s}{\alpha}\right) \qquad \text{(A1.2)}$$

Also it is likely that the autoconversion rate will increase with increasing vertical velocity. Therefore if we assume that the amount of cloud depends upon the vertical velocity, we can attempt to introduce this dependence by using a time constant inversely proportional to α ; we then have

$$P_a = \frac{\alpha}{\tau_a}\left(c - \frac{\ell r_s}{\alpha}\right) \qquad \text{(A1.3)}$$

The value chosen for τ_a is that suggested by Kessler, $\tau_a = 10^3 s$, and we use $\ell = 0.07$.

Figure A1(a) shows P_a derived from (A1.3) with $\alpha = 1$, and also from Kessler's formulation given by (A1.1). Also shown is the theoretical estimate due to Manton and Cotton (1977) which may be written as

$$P_a = \frac{c^{7/3}}{\tau_a} \qquad \tau_a = 1440 s \qquad c > 0.42$$

The similarity between the three curves is encouraging.

2. Collection

Kessler (1969) derived an expression for the collection rate which may be written as

$$P_c = 0.318 E N_0^{1/8} c (m \rho_0 F)^{7/8} F^{-1/2}$$

where $N_0 = 0.8 \times 10^{-7} m^{-4}$ is a parameter related to the drop-size spectrum, $E = 0.5$ is the collection efficiency and $F = \rho / \rho_0$ with $\rho_0 = 1.2$ kg m^{-3}

It is convenient to change the exponent of $(m \rho_0 F)$ from 7/8 to 1, so we have

$$P_c = \frac{1}{\tau_c} c m F^{1/2} \qquad \tau_c = 310 s$$

However thick clouds tend to produce more rain than thin ones and so we replace τ_c by τ_c / α giving

$$P_c = \frac{\alpha}{\tau_c} c m F^{1/2} \qquad \text{(A1.4)}$$

3. The determination of $\bar{m}$

From (A1.3) and (A1.4) we have

$$\bar{P} = \bar{P}_a + \bar{P}_c = \frac{\alpha}{\tau_a} (\bar{c} - \ell \bar{F}_s) + \frac{\bar{c} \bar{m}}{\tau_c} F^{1/2} \qquad \text{(A1.5)}$$

In order to use this we must derive $\bar{m}$. Assume there is no storage of rain-water $\left(\frac{d\bar{m}}{dt} = 0 \right)$ so that the continuity equation for $\bar{m}$ becomes

$$\frac{\partial}{\partial p} (\omega_t \bar{m}) = \bar{P} \qquad \text{(A1.6)}$$

where ω_t is taken to be a representative terminal velocity for raindrops. We now split (A1.6) into two parts which give the changes in $\bar{m}$ due to autoconversion and collection in a layer Δp , these are

$$\Delta\bar{m}_a = \frac{\bar{P}_a \Delta p}{\omega_t} \qquad \Delta\bar{m}_c = \frac{\bar{P}_c \Delta p}{\omega_t} \qquad \text{(A1.7)}$$

We now assume that only the rainwater formed in a given layer by autoconversion takes part in the collection process; substituting $\Delta\bar{m}_a$ for $\bar{m}$ in the expression for $\bar{P}_c$ then gives

$$\bar{P}_c = \bar{P}_a \frac{\bar{c}\,\Delta p}{\tau_c \omega_t} F^{1/2} \qquad \bar{P} = \bar{P}_a \left(1 + \frac{\bar{c}\,\Delta p}{\tau_c \omega_t} F^{1/2}\right)$$

Therefore we have a local conversion rate and the effect of the collection is to lead to an enhancement of the autoconversion rate which depends upon the amount of cloud liquid water. Using $\tau_c = 310\,s$, $\omega_t = 0.6F^{1/2}_{mb}\,s^{-1}$ and $\Delta p = 100\,mb$ we have

$$\bar{P} = \bar{P}_a(1 + 0.538\,\bar{c}F^{-1/2}) \text{ or } P = P_a(1 + 0.538\,c\alpha F^{-1/2}) \qquad \text{(A1.8)}$$

The procedure described here minimises the collection rate by assuming that none of the rain falling through a layer takes part in the collection process. An alternative strategy is to assume that all the rain from above falls through the cloud in the layer below; this is equivalent to assuming that the cloud in a layer is distributed uniformly in the horizontal. The first procedure will underestimate the rain from several adjacent cloudy layers whereas the second will overestimate the likely collection when rain formed at higher levels falls through relatively cloudless layers. In this study we use the first approach because it is convenient to have a purely local conversion rate.

Figure A1(b) shows the total conversion rate derived from (A1.8) with $\alpha = 1$. Also shown is the expression used by Jonas

$$P = \frac{1}{\tau}(c - 0.15\Gamma_s) \qquad \text{(A1.9)}$$

with $\tau = 720\,s$

It is unclear which of these is the best formulation, but (A1.8) does have the advantage of a better theoretical foundation than (A1.9).

Figure A1(c) illustrates the effect of varying the amount of cloud α when (A1.8) is used in conjunction with (A1.3). The results are consistent with the fact that it is easier for thick clouds to produce rain than thin ones, but the detailed behaviour of τ_a and P is rather speculative.

In this study (A1.3) and (A1.8) have been used to parameterise the cloud physics. However later experiments indicated that we get reasonable results if we neglect collection and remove the α dependence of the autoconversion time constant; that is it may be sufficient to use

$$P = \frac{1}{\tau_a}\left(c - \frac{l r_s}{\alpha}\right)$$

Appendix 2

J used the statistical distribution of 850 mb humidity observations, and the corresponding distribution for wet occasions, to verify his parameterisation scheme. An alternative approach is to use these statistics to estimate the autoconversion threshold. We consider four forms of the threshold, each expressed in terms of the relative humidity.

(i) $k\bar{r}_s$ - Jonas (1976) (ii) $\ell\bar{r}_s/\alpha$ - Modified Jonas

(iii) $m/\ell\bar{r}_s$ - Kessler (1969) (iv) $n/\ell\bar{r}_s\alpha$ - Modified Kessler

Here (ii) and (iv) are derived from (i) and (iii) by assuming that the threshold is inversely proportional to α

In the following analysis the S-D method is used although from the results it is easy to derive the appropriate expressions for the J method.

We assume that in a grid box $H_L = w/\bar{r}_{sL}$ is distributed normally about its mean value $\bar{H}_L$ with a standard deviation σ_s ; the probability function is then

$$P_s(H_L, \bar{H}_L) = \frac{1}{\sqrt{2\pi}\,\sigma_s} \exp\left[-\frac{(H_L - \bar{H}_L)^2}{2\sigma_s^2}\right] \qquad \text{(A2.1)}$$

Similarly we assume that $\bar{H}_L$ is distributed normally about a time mean $\hat{H}_L$ with standard deviation σ_t , so

$$P_t(\bar{H}_L, \hat{H}_L) = \frac{1}{\sqrt{2\pi}\,\sigma_t} \exp\left[-\frac{(\bar{H}_L - \hat{H}_L)^2}{2\sigma_t^2}\right] \qquad \text{(A2.2)}$$

Since observations are taken at different points in space and time, the probability of measuring a value of H_L is

$$P(H_L, \hat{H}_L) = \int_0^\infty P_s(H_L, \bar{H}_L)\, P_t(\bar{H}_L, \hat{H}_L)\, d\bar{H}_L$$

Using (A2.1) and (A2.2) then yields

$$P(H_L, \hat{H}_L) = \frac{1}{\sqrt{2\pi}\,\sigma} \exp\left[-\frac{(H_L - \hat{H}_L)^2}{2\sigma^2}\right]\left(\frac{1 + \mathrm{erf}(b)}{2}\right) \qquad \text{(A2.3)}$$

with $\sigma^2 = \sigma_s^2 + \sigma_t^2$ and $b = \frac{1}{\sqrt{2}\,\sigma_s\sigma_t}\left(\frac{\sigma_t^2 H_L + \sigma_s^2 \hat{H}_L}{\sigma}\right)$

Now consider the probability of H_L being observed when it is raining, $P_W(H_L,\hat{H}_L)$ say . If H_{LR} is the critical humidity at which rain starts, then

$$P_W(H_L,\hat{H}_L) = \int_{H_{LC}}^{\infty} P_S(H_L,\bar{H}_L)\, P_t(\bar{H}_L,\hat{H}_L)\, d\bar{H}_L$$

Integration shows that P_W is given by (A2.3) with b replaced by b_W , where

$$b_W = \frac{1}{\sqrt{2}\sigma_t\sigma_s}\left(\frac{\sigma_t^2 H_L + \sigma_s^2 \hat{H}}{\sigma} - \sigma H_{LR}\right)$$

The statistics for P and P_W will be unreliable because of inaccuracies in humidity observation, however $\mathcal{J} = P/P_W$ should be relatively free of error. We now assume that

(a) $H_L - H$ is usually small so we can replace H_L by H

(b) $\sigma_S = \sigma_t = \sigma_{HL}$

$\mathcal{J}$ then becomes

$$\mathcal{J} = \frac{1 + \mathrm{erf}[(H+\hat{H})/2\sigma_{HL}]}{1 + \mathrm{erf}[(H+\hat{H}-2H_R)/2\sigma_{HL}]} \qquad \text{(A2.4)}$$

When the J scheme is used $\mathcal{J}$ is still given by this expression with σ_{HL} replaced by σ_H . Table A1 shows $\mathcal{J}$ as a function of relative humidity.

The observed $\mathcal{J}$ is known as a function of relative humidity whereas (A2.4) is expressed in terms of total relative humidity. Therefore we assume that at a point the relationship between relative humidity and total relative humidity is the same as that given by the subgridscale condensation scheme; this allows us to turn observed relative humidities into "observed" total relative humidities Knowing $\mathcal{J}$ and H , and using a value of $\hat{H}$ which corresponds to a relative humidity of 0.775, (A2.4) can be solved for H_c . From this we deduce the corresponding cloud liquid water relative humidity and from this we compute k, ℓ, m and n

Figure A2 shows various estimates of the threshold parameters (we use the same notation (i)/(ii) as in Section 8). When J/J is used k tends to decrease with increasing relative humidity; the variability of k indicates that using J/J with a constant k type of threshold cannot reproduce the statistical distribution

of 850 mb observations. Also shown in Figure A2(a) are estimates of k and ℓ using S/R. The relative constancy of these is encouraging and indicates that suitable values of k and ℓ be in the range 0.10 - 0.12 and 0.05 - 0.08 respectively. Examination of the initialised rainfall coverage using k and ℓ in these ranges showed that

(a) the coverage was not very sensitive to the choice of ℓ and that ℓ = 0.07 gave reasonable results,

(b) the coverage was sensitive to the choice of k and that the use of k = 0.12 gave similar results to ℓ = 0.07.

Therefore these results indicate that with the S/R combination it is appropriate to use a modified Jonas type threshold with ℓ = 0.07.

Figure A2(b) shows that we get relatively constant values of m and n with the S/R combination. The mean value of m is 0.82 which is higher than the value of 0.5 suggested by Kessler. However the introduction of an α dependence in the threshold gives a mean value of 0.48; the closeness of this to Kessler's suggestion adds weight to the argument for introducing an α dependence into the threshold.

References

Burridge, D M and A J Gadd — 1977 — "The Meteorological Office operational 10-level numerical weather predition model (Dec 1975)." London Met Office, Sci Paper No 34.

Jonas, P R — 1976 — " A revised parameterisation of the condensation and precipitation processes for use in numerical forecasting models." Met O 11 Tech Note No 67.

Kessler, E — 1969 — "On the distribution and continuity of water substance in atmospheric circulations." Met Monograph, 10, No 32, Americal Meteorological Societ

Louis, J F — 1977 — "A case study of air mass transformation." ECMWF Seminar 1977, 357-373.

Manton, M J and W R Cotton — 1977 — "Formulation of approximate equations for modelling moist deep convection on the Mesoscale." Ats Sc Paper No 266, Dept Ats Sc, Colorado State University

Mellor, G L — 1977 — "The gaussian cloud model relations." J Ats Sc, 34, 356-358.

Ricketts, J N — 1973 — "An investigation into a relationship between upper relative humidity and cloud cover." Met Mag, 102, 146-156.

Sommeria, G and J W Deardorff — 1977 — "Subgridscale condensation in models of non-precipitating clouds." J Ats Sc, 34, 344-355.

Wickham, P G — 1977 — "Errors in rainfall forecasts by the 10-level model 1973-1977." Met O 11 Tech Note No 99.

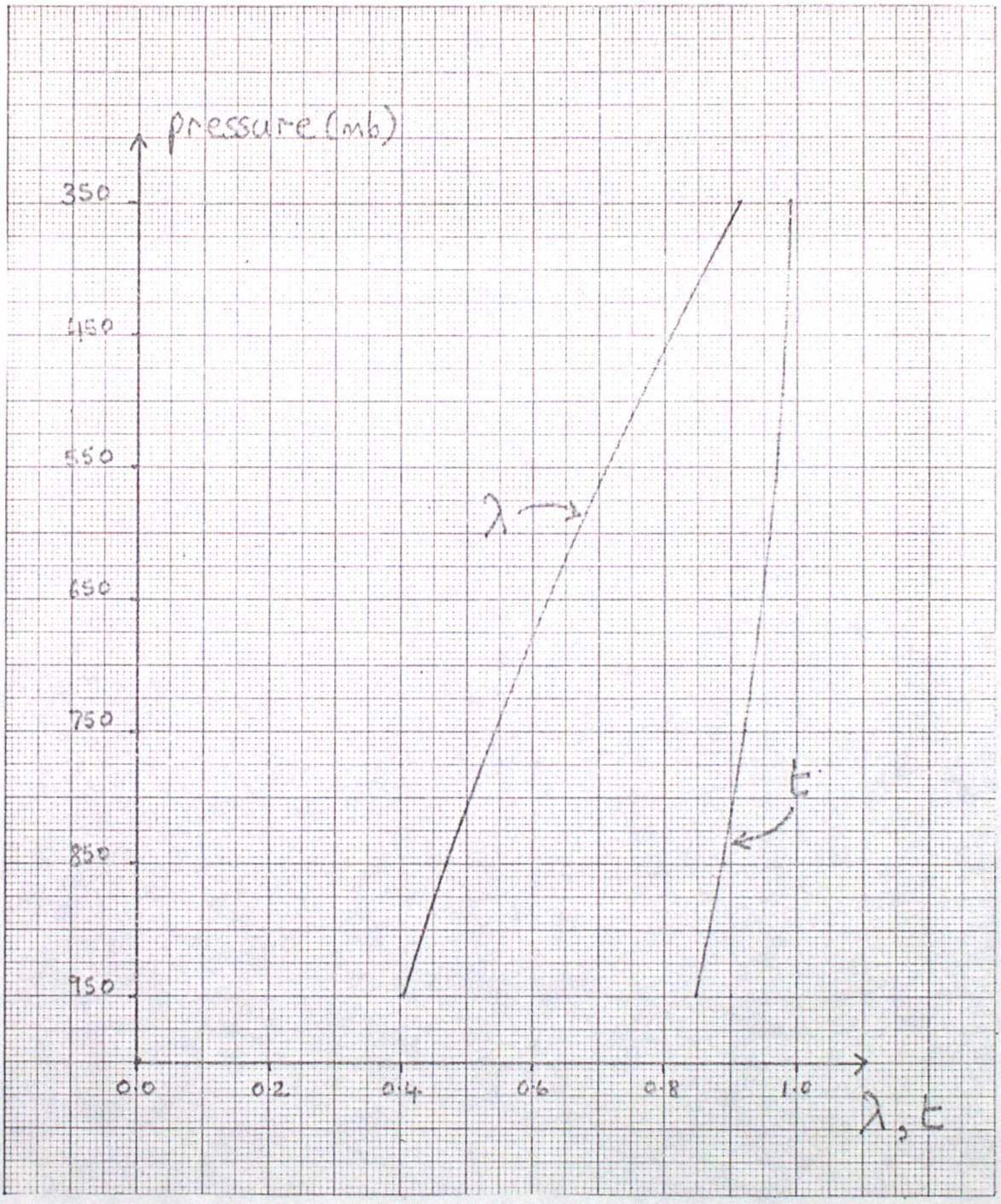

Figure 1

λ and t for an ICAO atmosphere with $\bar{c}/\bar{r}_s = 10\%$

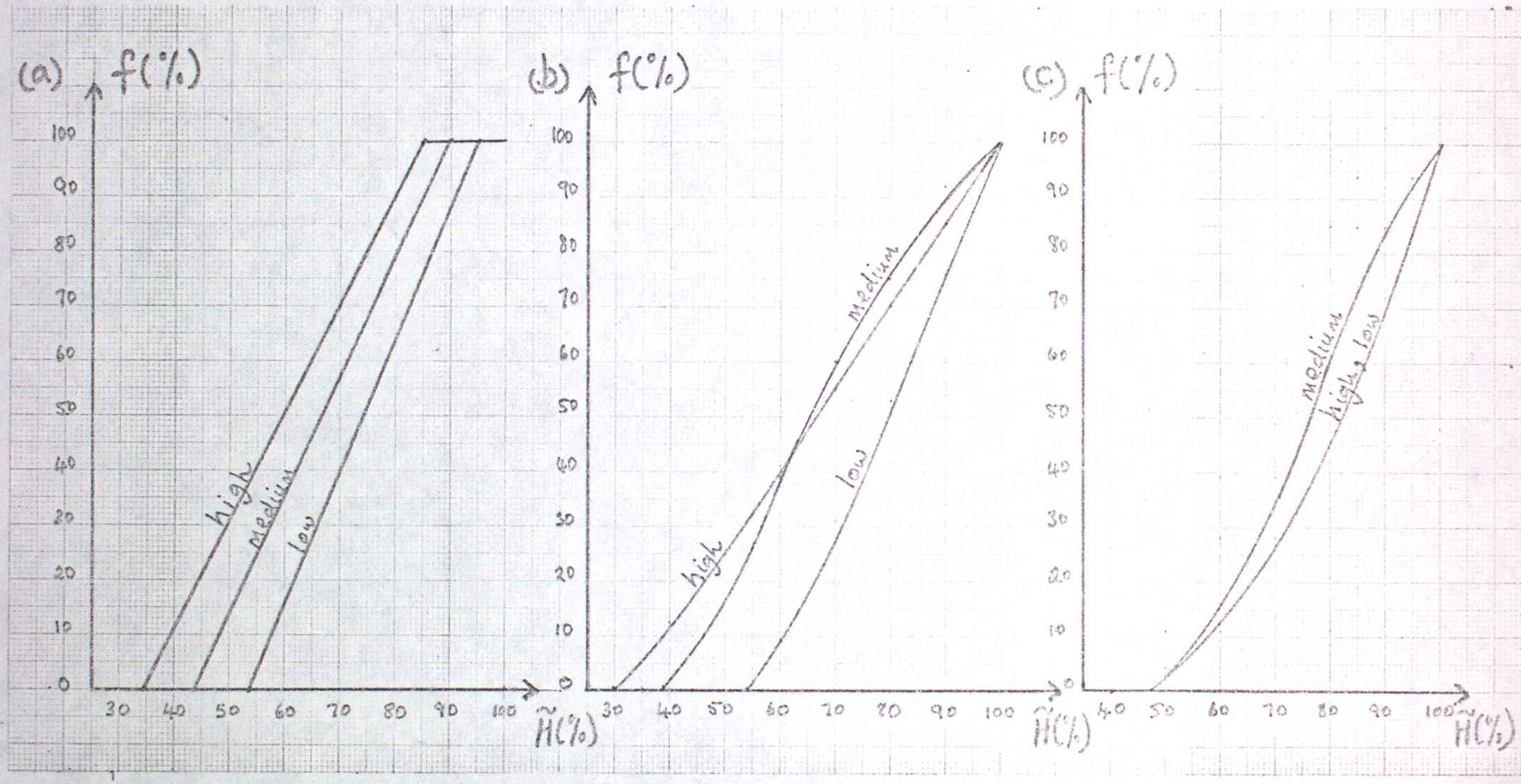

Figure 2

Fractional cloud cover derived by assuming that the relative humidity is uniform in each cloud layer.

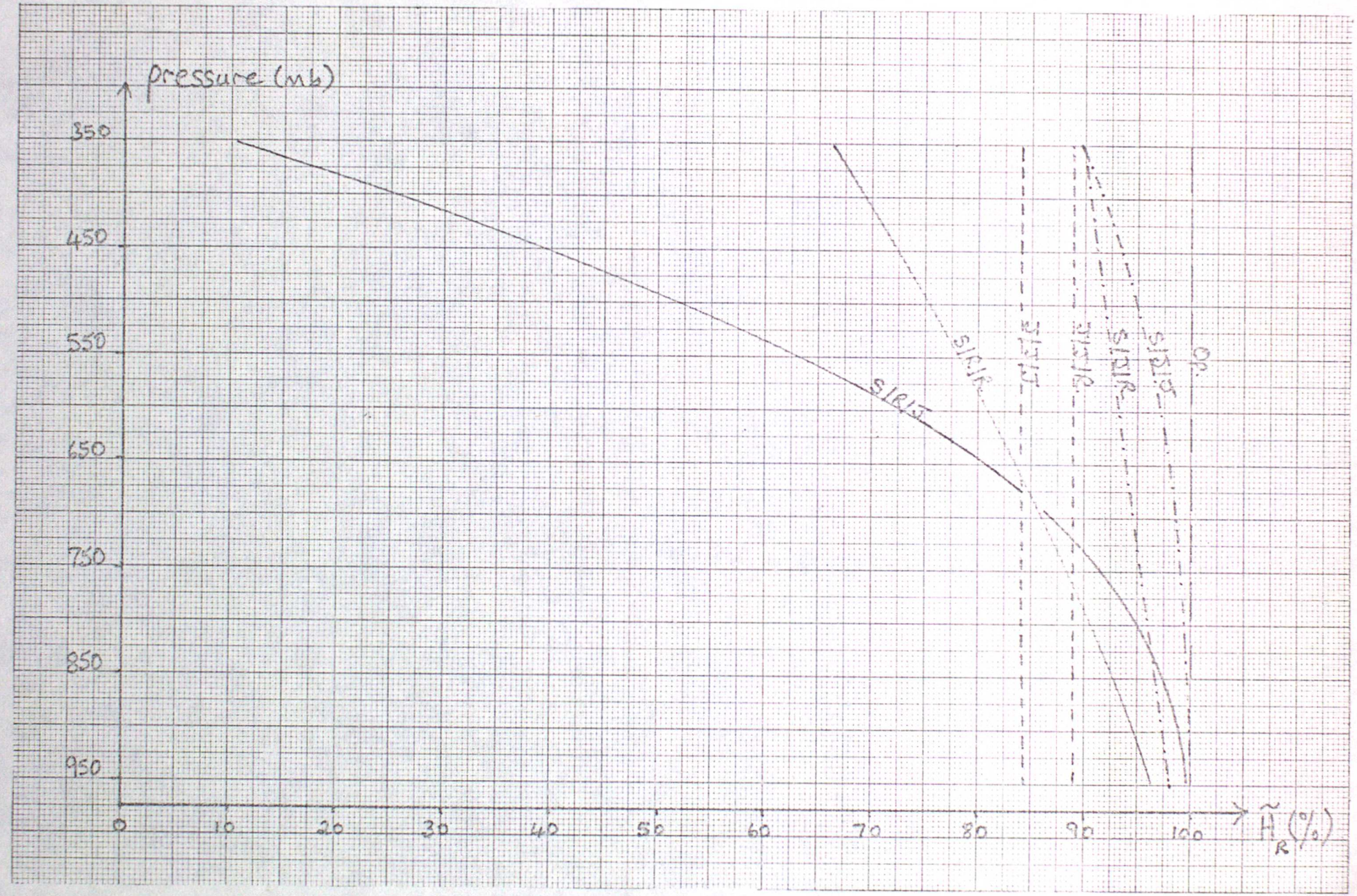

Figure 3

Relative humidity at which rain forms ($\tilde{H}_R$) for various condensation schemes

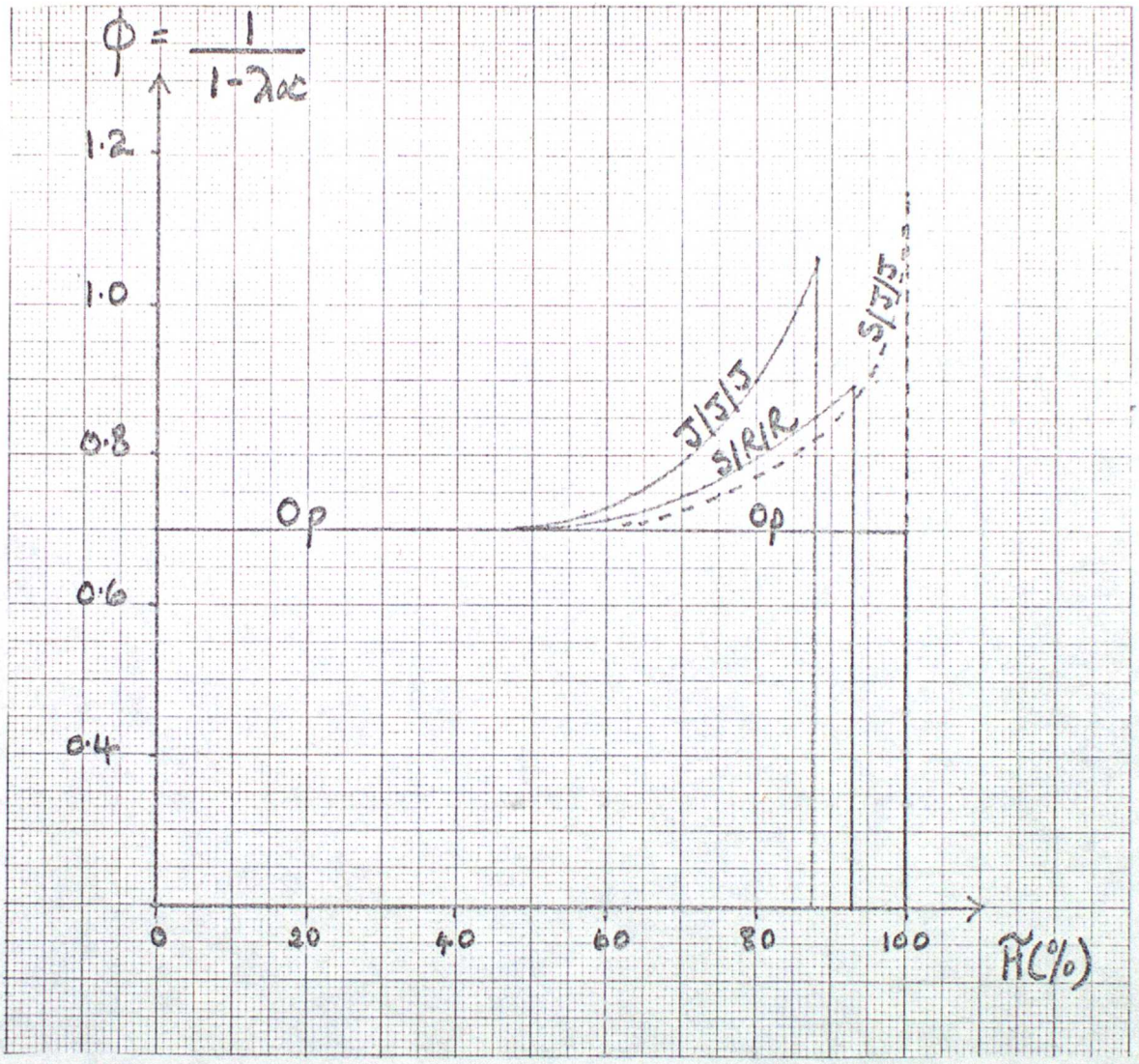
$\phi = \frac{1}{1-\lambda\alpha}$
1·2
1·0
0·8
0·6
0·4
0p
0p
J/J/J
S/R/R
S/J/J
0
20
40
60
80
100
R(%)

Figure 4

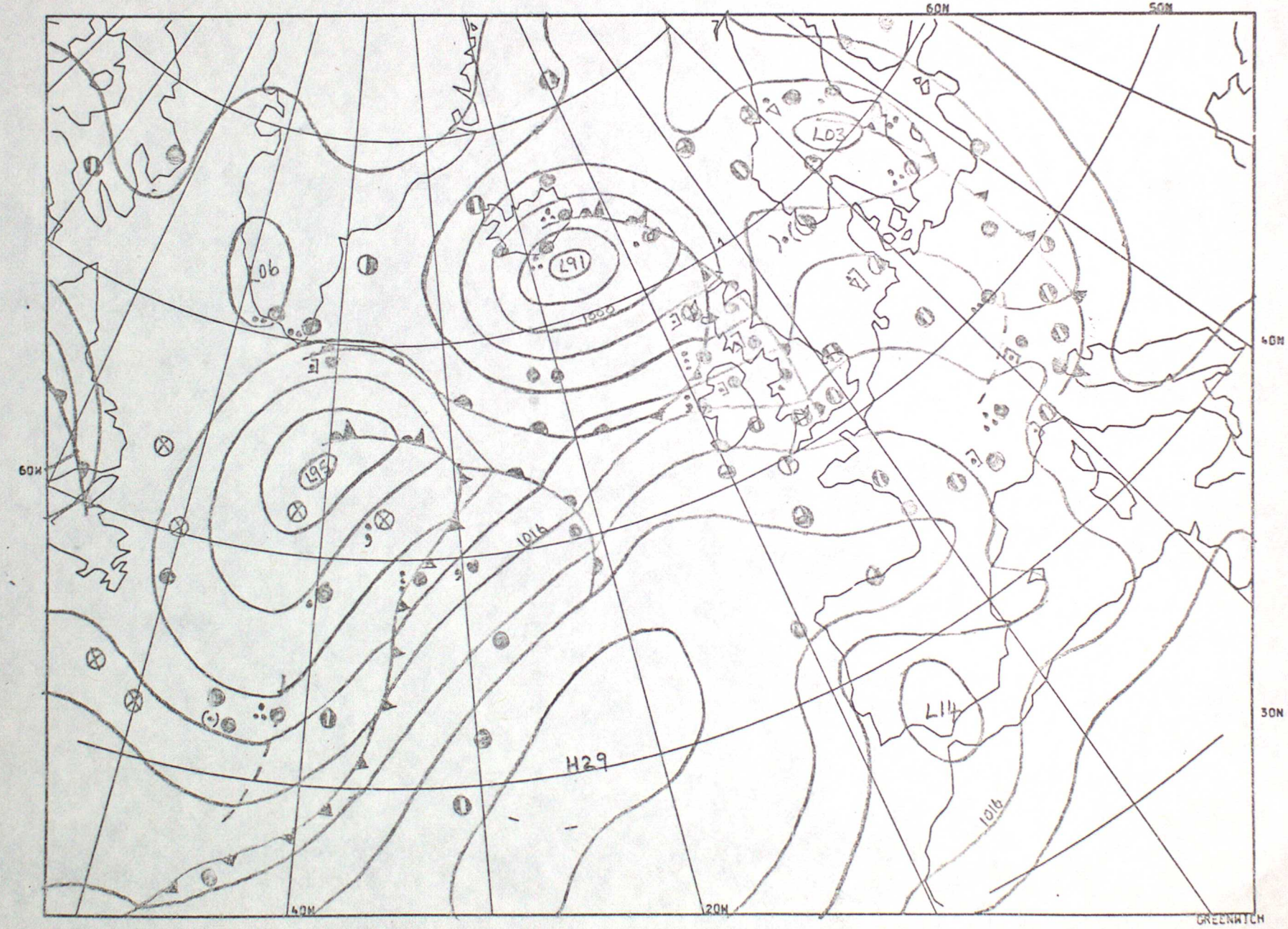

Figure-5 - surface analysis- at-00z -30/6/77

FORECAST SURFACE PRESSURE AND PRECIPITATION

12HOUR FORECAST.DATA TIME=12Z 29/6/77.VERIFICATION TIME=0Z 30/6/77

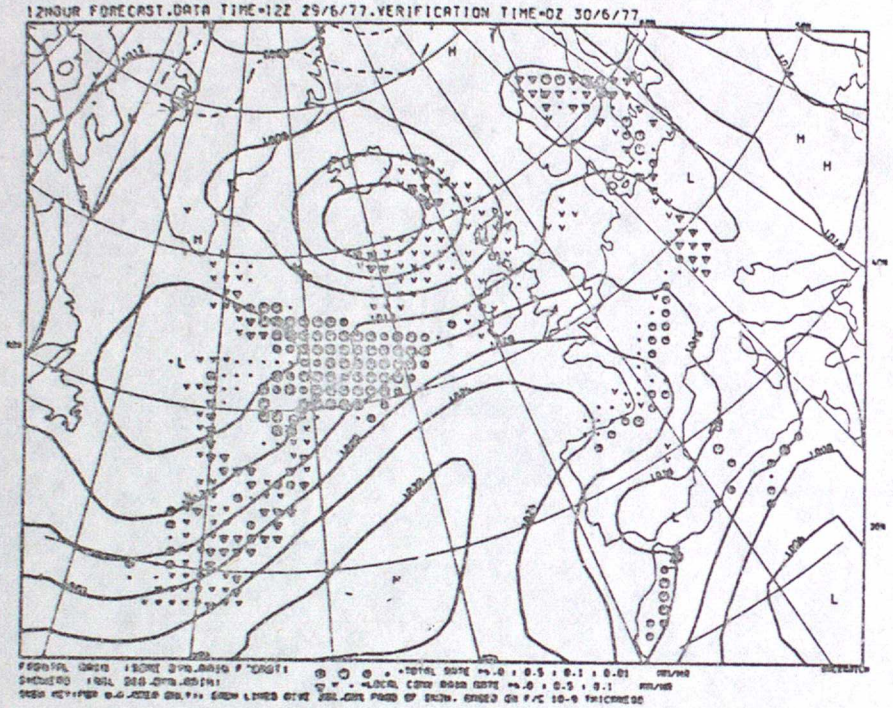

RATE OF DYNAMIC RAIN ISOPLETHS AT 0.5 MM/HR

12HOUR FORECAST.DATA TIME=12Z 29/6/77.VERIFICATION TIME=0Z 30/6/77

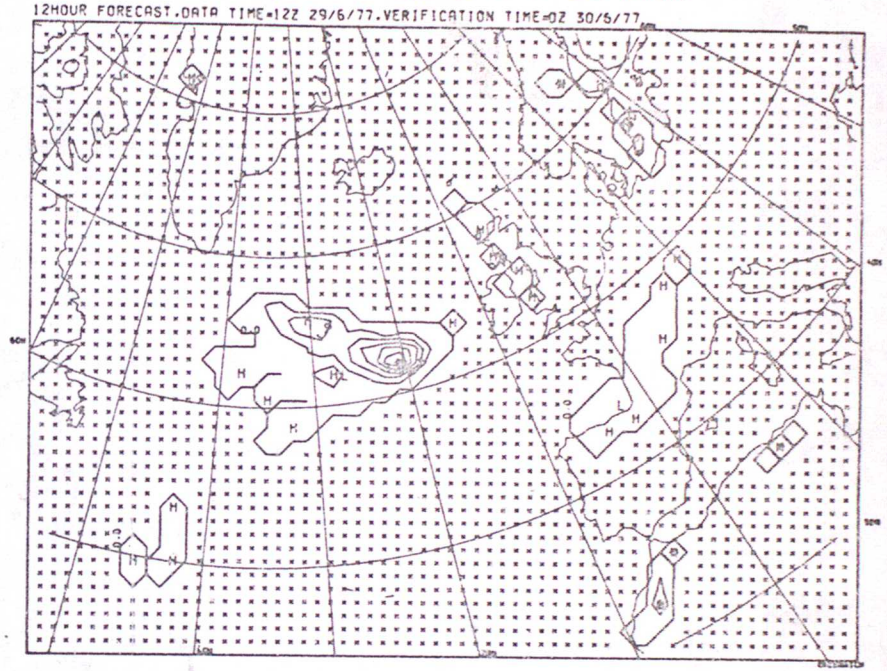

TOTAL RATE OF RAIN 0.5 MM ISOHYET INTERVAL

12HOUR FORECAST.DATA TIME=12Z 29/6/77.VERIFICATION TIME=0Z 30/6/77

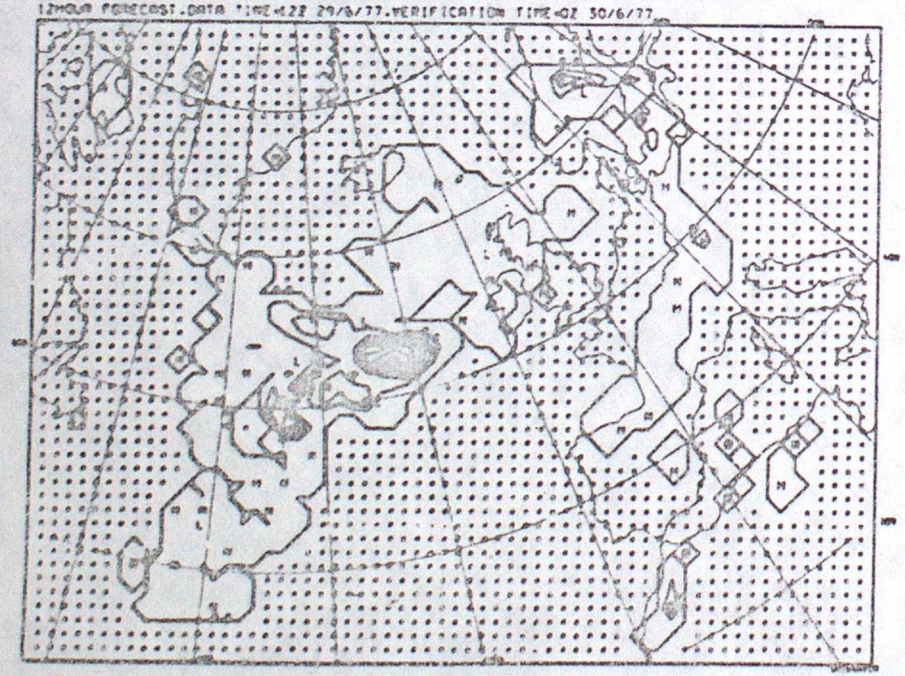

RATE OF CONVECTIVE RAIN ISOPLETH AT 0.25 MM/HR

12HOUR FORECAST.DATA TIME=12Z 29/6/77.VERIFICATION TIME=0Z 30/6/77

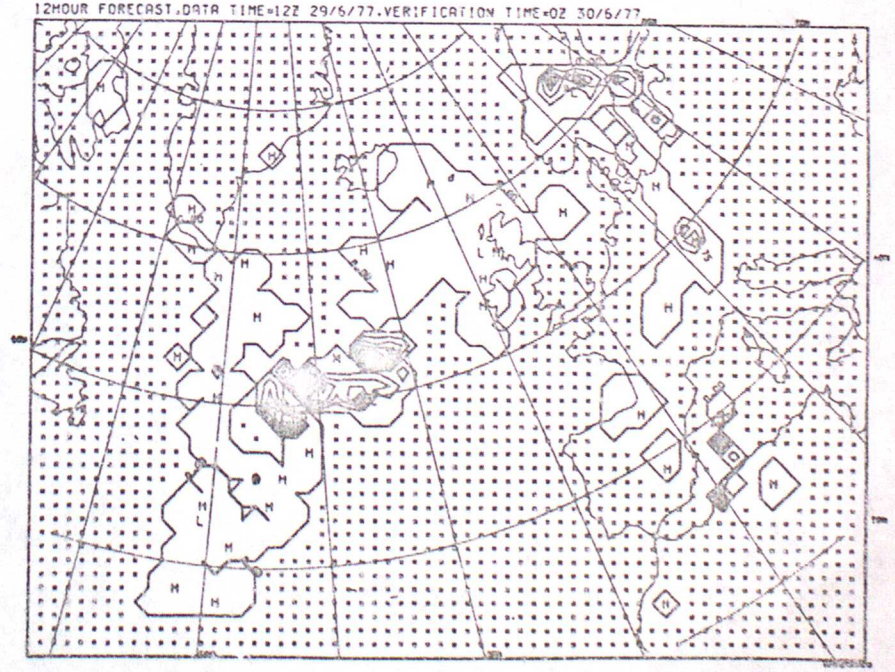

Figure 6 - 12 hour forecast (V.T. 00Z 30/6/77)

(a)

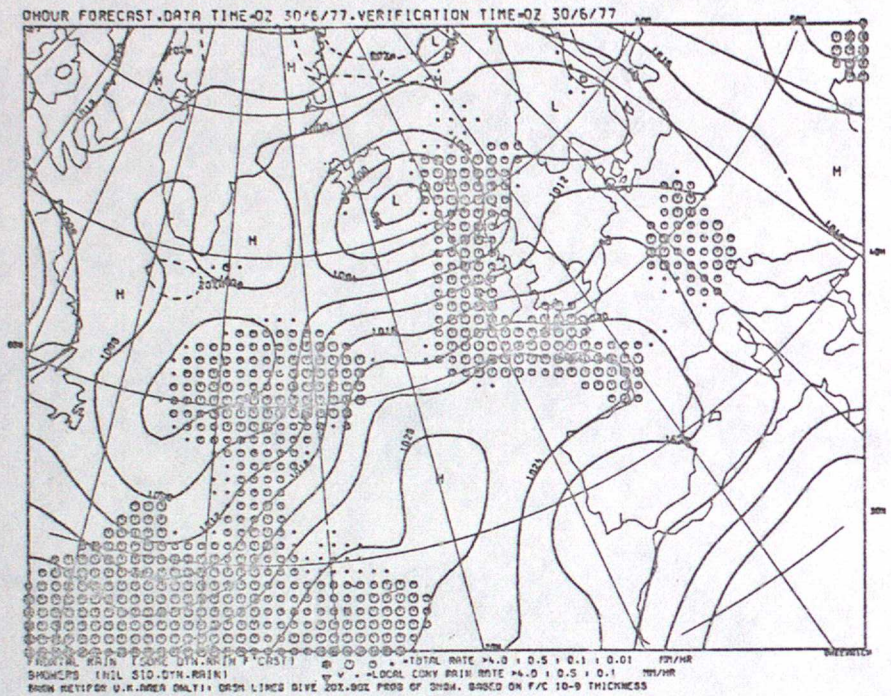

(b)

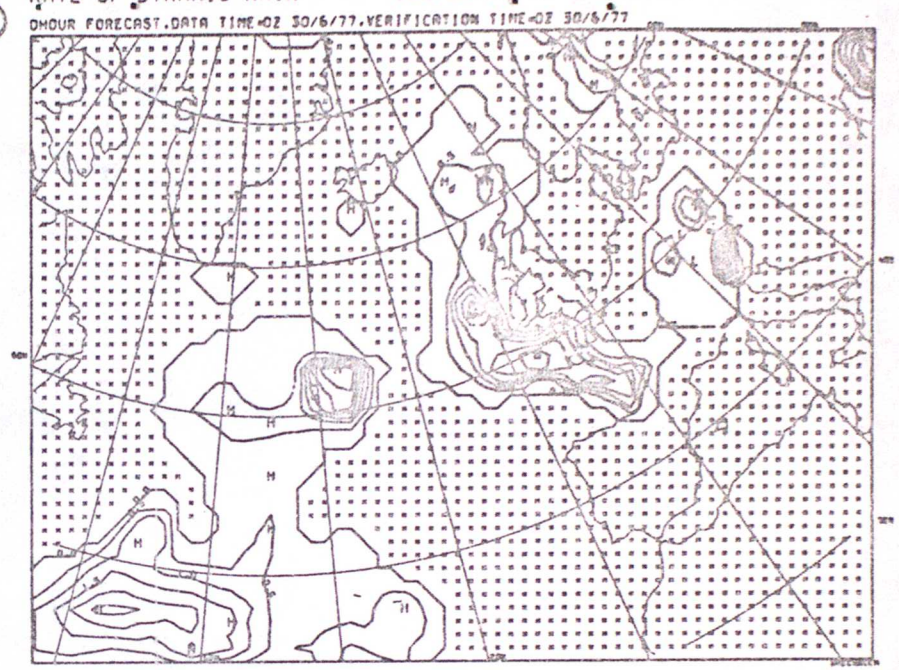

(c)

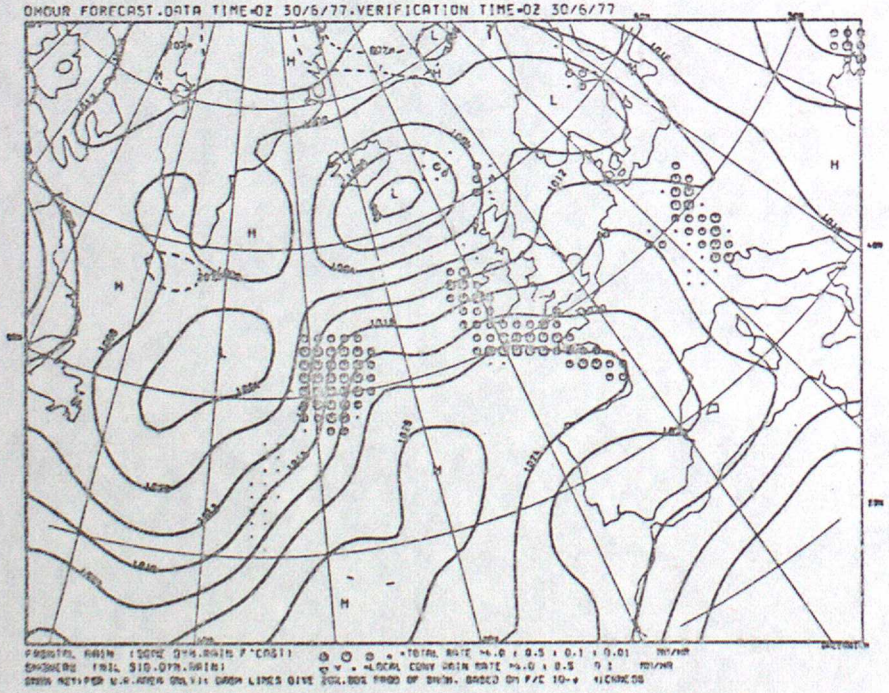

(d)

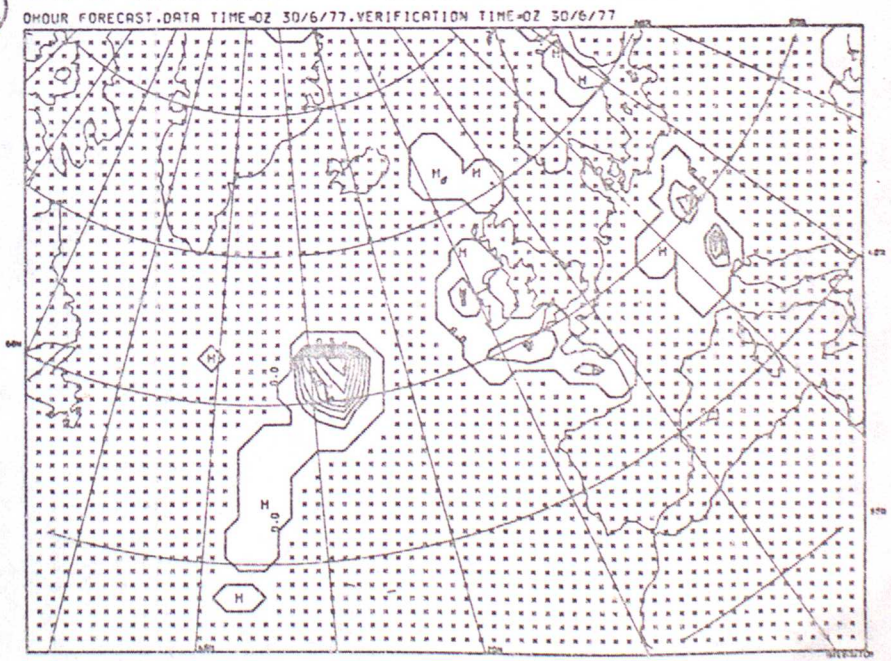

Figure 7 - Initialised rain rates using J/J/J (a and b) and S/R/R (c and d)

FORECAST SURFACE PRESSURE AND PRECIPITATION

6HOUR FORECAST.DATA TIME=0Z 30/6/77.VERIFICATION TIME=6Z 30/6/77

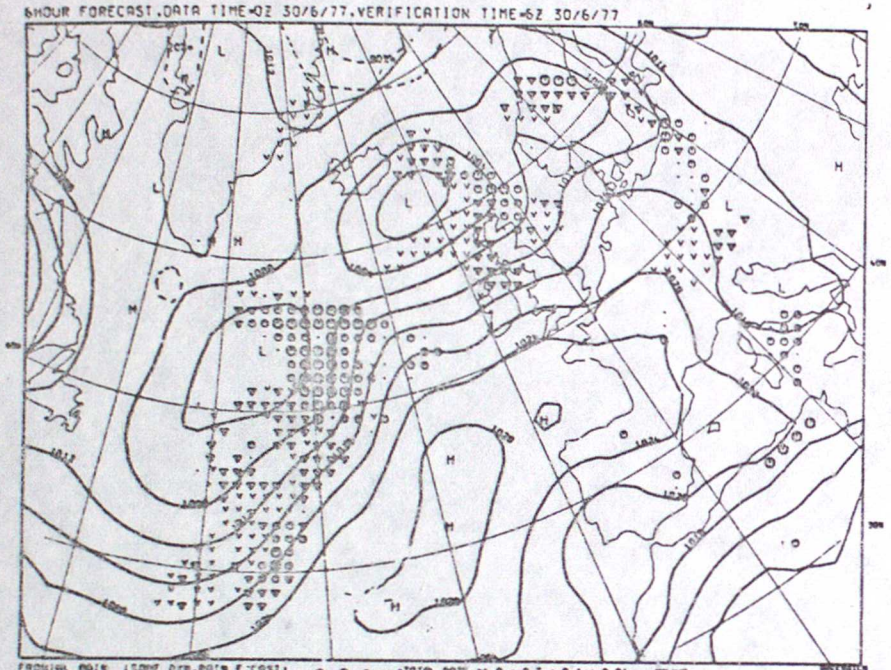

RATE OF DYNAMIC RAIN ISOPLETHS AT 0.5 MM/HR

6HOUR FORECAST.DATA TIME=0Z 30/6/77.VERIFICATION TIME=6Z 30/6/77

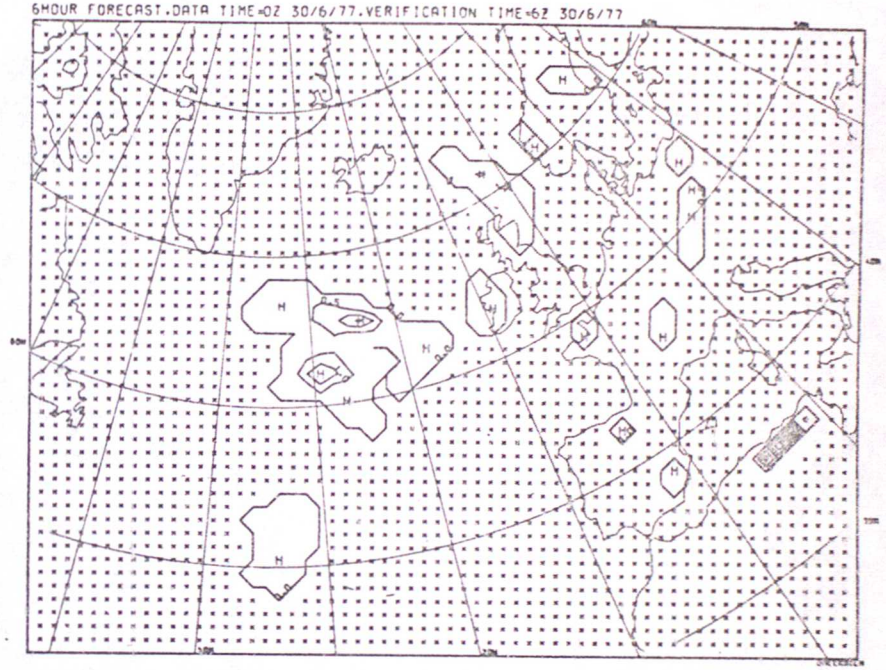

ACC. CONVECTIVE RAIN ISOHYETS AT 0.5 MM INTERVALS

6HOUR FORECAST.DATA TIME=0Z 30/6/77.VERIFICATION TIME=6Z 30/6/77

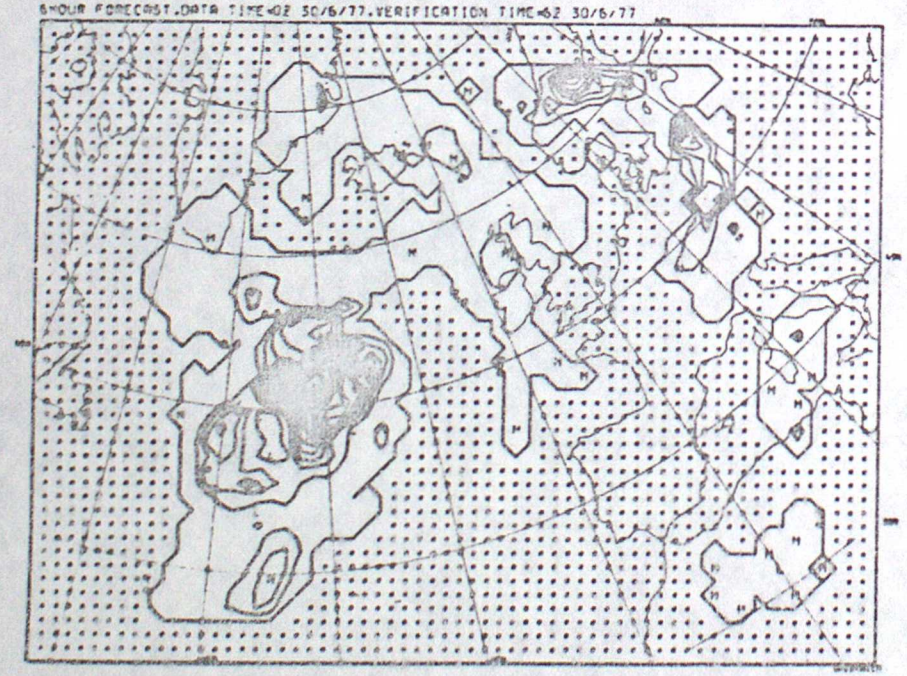

ACCUMULATED RAIN ISOHYETS AT 2 MM INTERVALS

6HOUR FORECAST.DATA TIME=0Z 30/6/77.VERIFICATION TIME=6Z 30/6/77

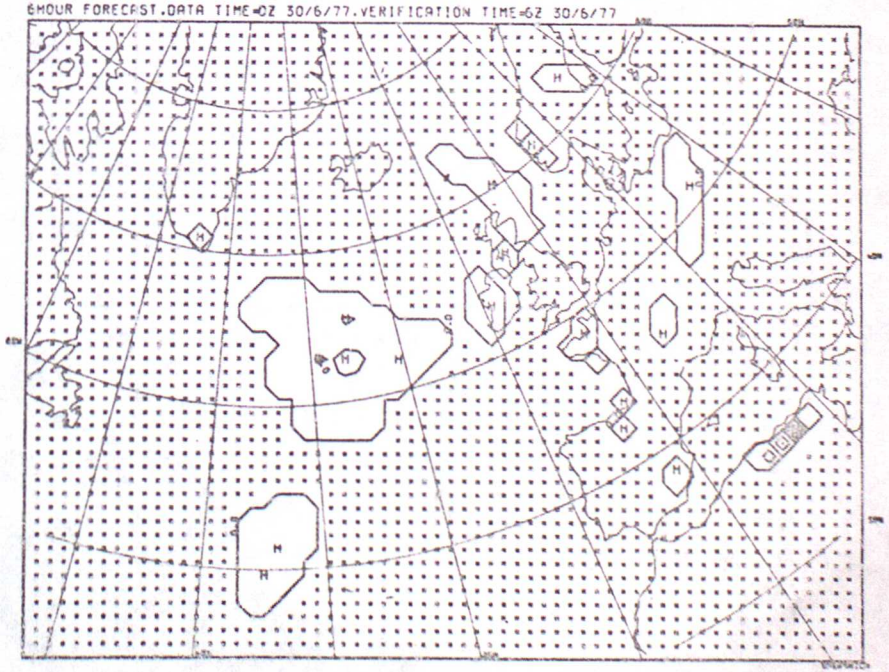

Figure 8 - 6 hour forecast using the operational condensation scheme.

FORECAST SURFACE PRESSURE AND PRECIPITATION

6HOUR FORECAST.DATA TIME=0Z 30/6/77.VERIFICATION TIME=6Z 30/6/77

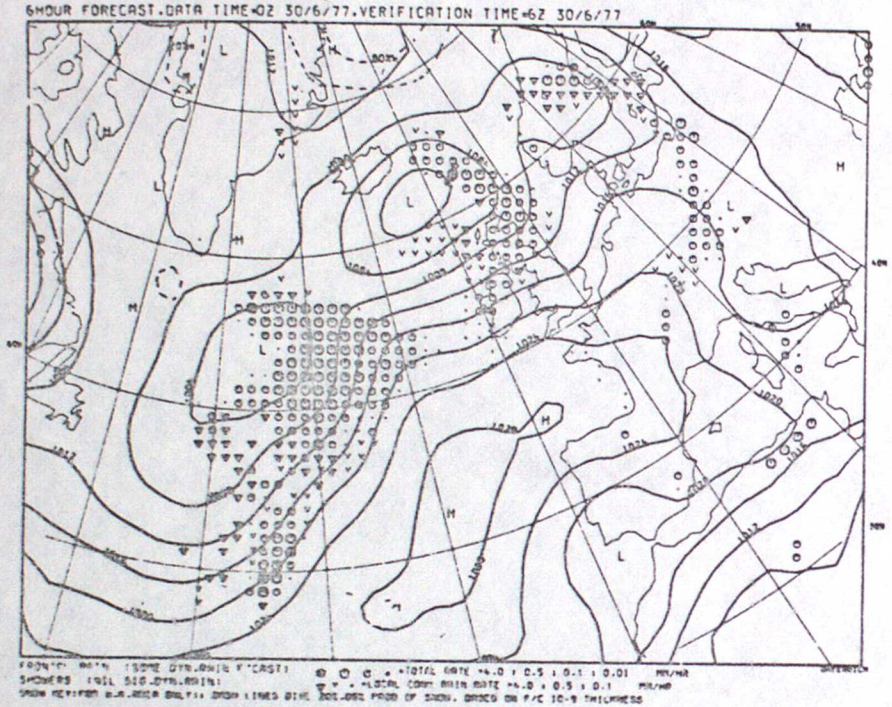

RATE OF DYNAMIC RAIN ISOPLETHS AT 0.5 MM/HR

6HOUR FORECAST.DATA TIME=0Z 30/6/77.VERIFICATION TIME=6Z 30/6/77

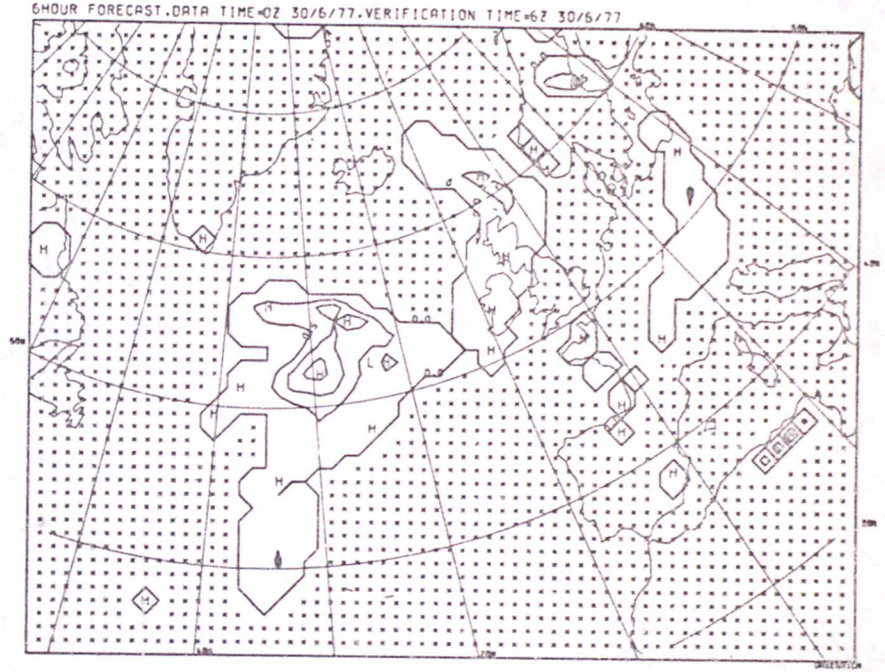

ACC. CONVECTIVE RAIN ISOHYETS AT 0.5 MM INTERVALS

6HOUR FORECAST.DATA TIME=0Z 30/6/77.VERIFICATION TIME=6Z 30/6/77

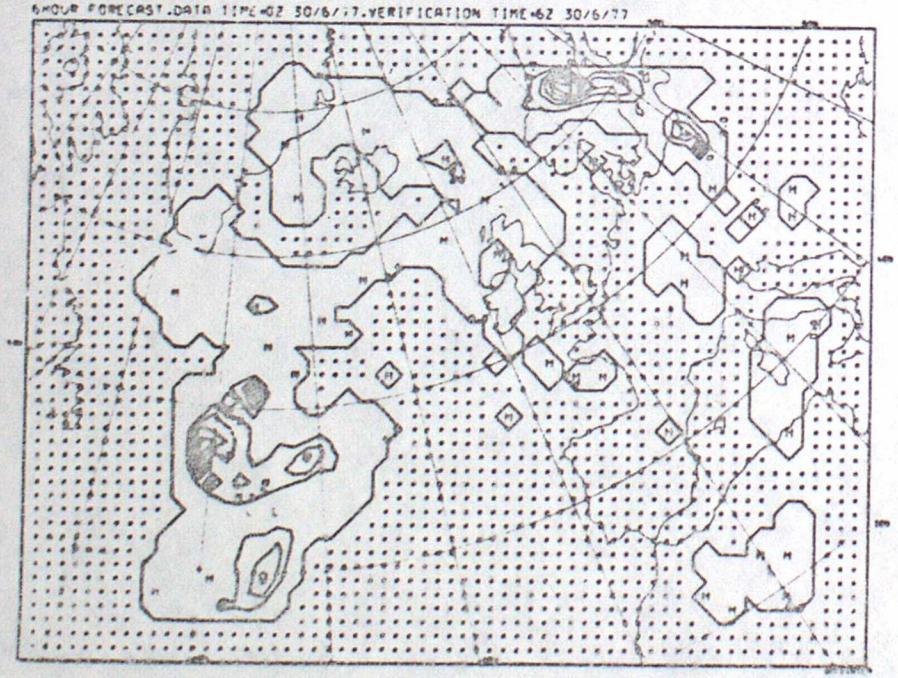

ACCUMULATED RAIN ISOHYETS AT 2 MM INTERVALS

6HOUR FORECAST.DATA TIME=0Z 30/6/77.VERIFICATION TIME=6Z 30/6/77

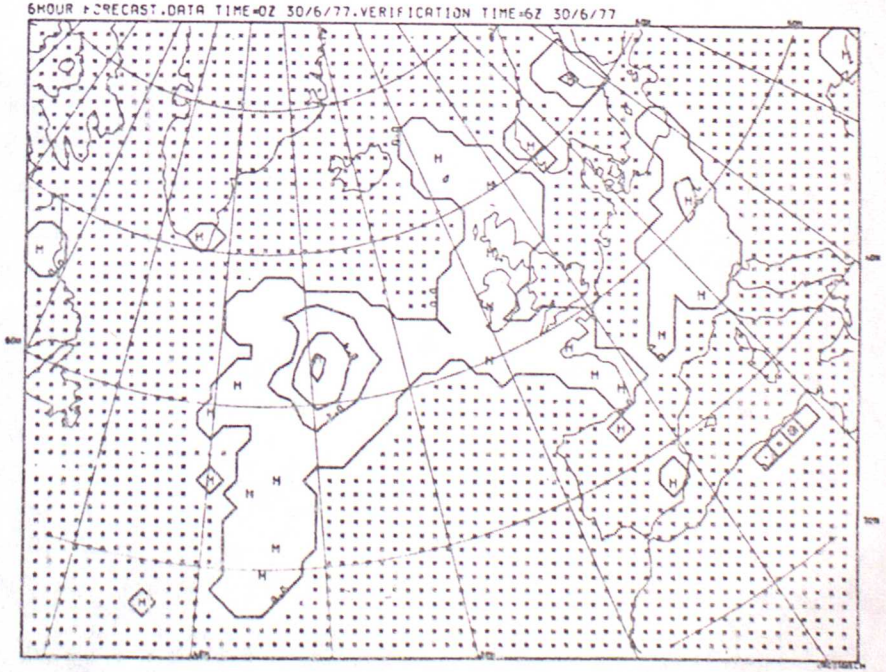

Figure 9 - 6 hour forecast using the S/R/R condensation scheme

FORECAST SURFACE PRESSURE AND PRECIPITATION

6HOUR FORECAST.DATA TIME=0Z 30/6/77.VERIFICATION TIME=6Z 30/6/77

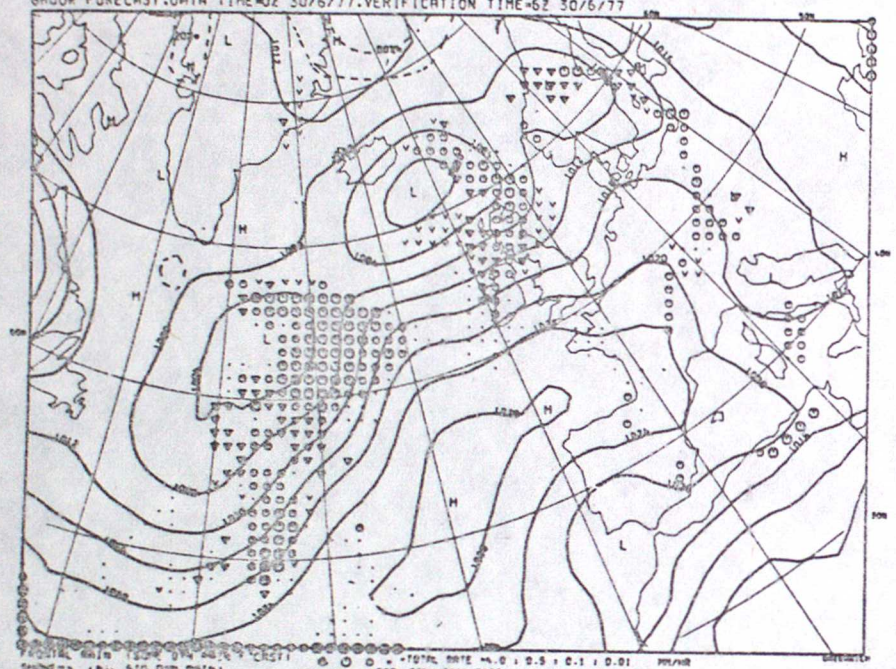

RATE OF DYNAMIC RAIN ISOPLETHS AT 0.5 MM/HR

6HOUR FORECAST.DATA TIME=0Z 30/6/77.VERIFICATION TIME=6Z 30/6/77

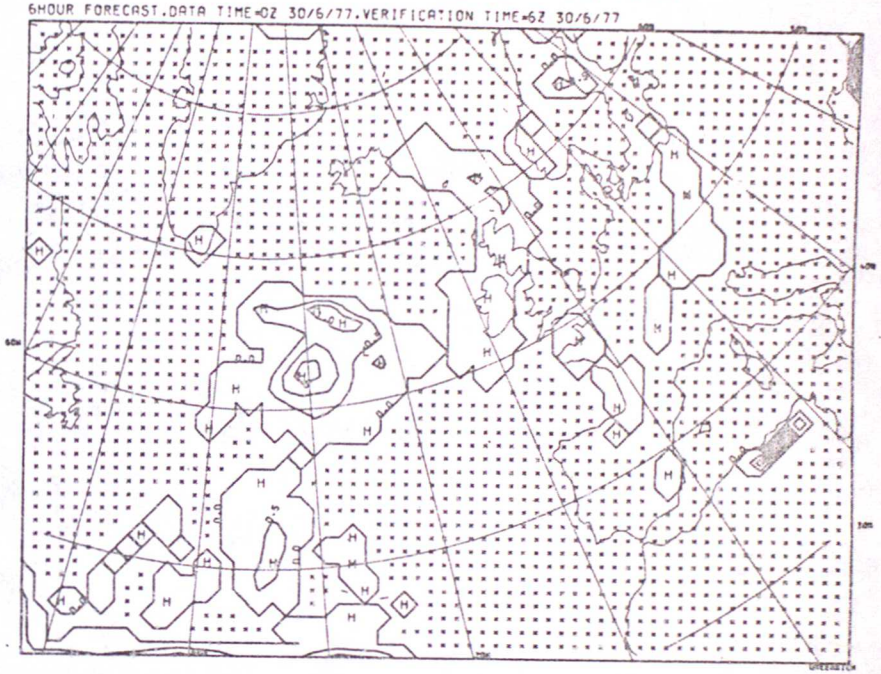

ACC. CONVECTIVE RAIN ISOHYETS AT 0.5 MM INTERVALS

6HOUR FORECAST.DATA TIME=0Z 30/6/77.VERIFICATION TIME=6Z 30/6/77

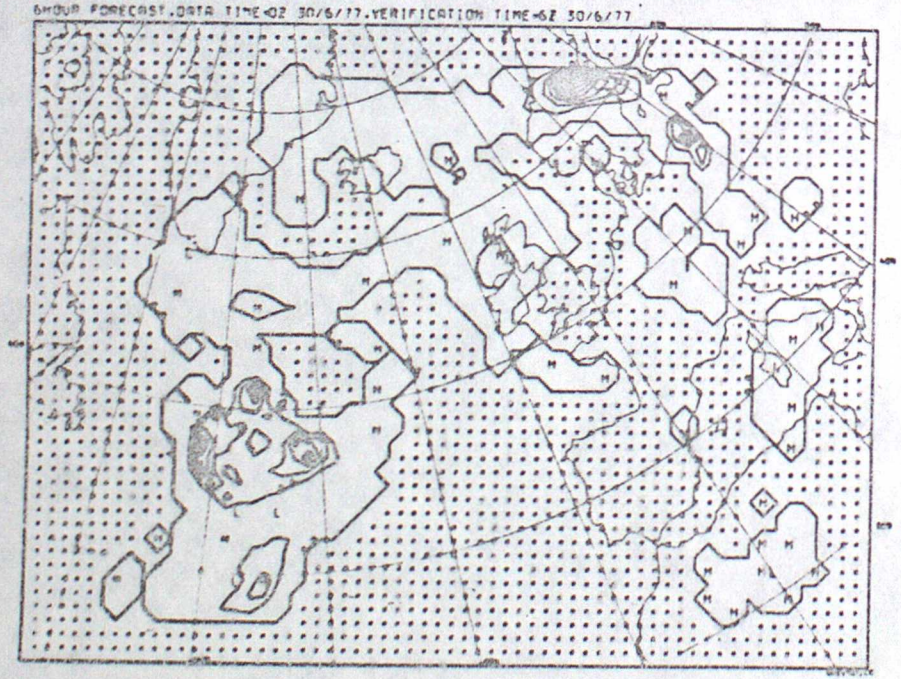

ACCUMULATED RAIN ISOHYETS AT 2 MM INTERVALS

6HOUR FORECAST.DATA TIME=0Z 30/6/77.VERIFICATION TIME=6Z 30/6/77

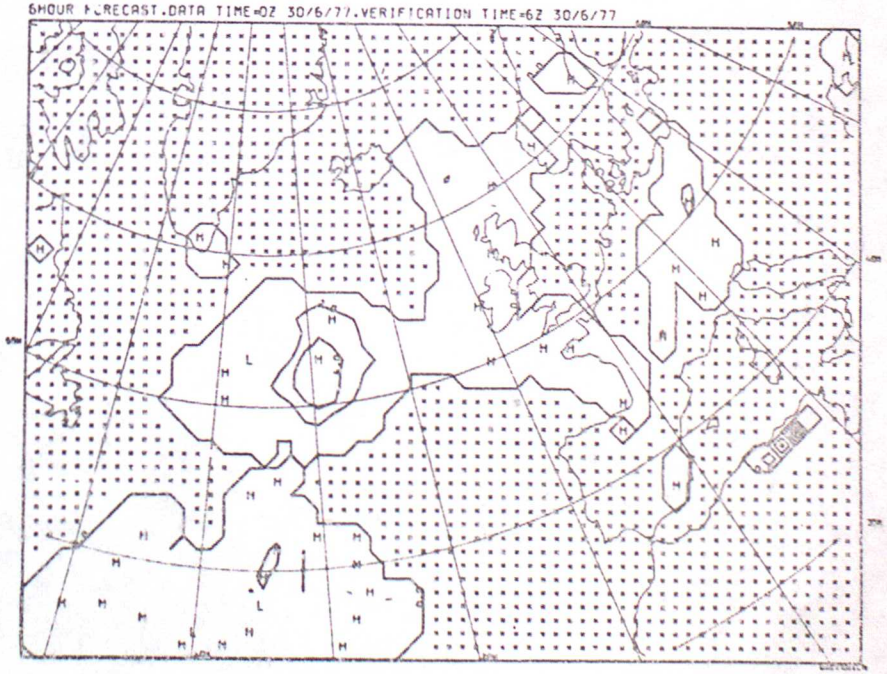

Figure 10 - 6 hour forecast using the J/J/J condensation scheme

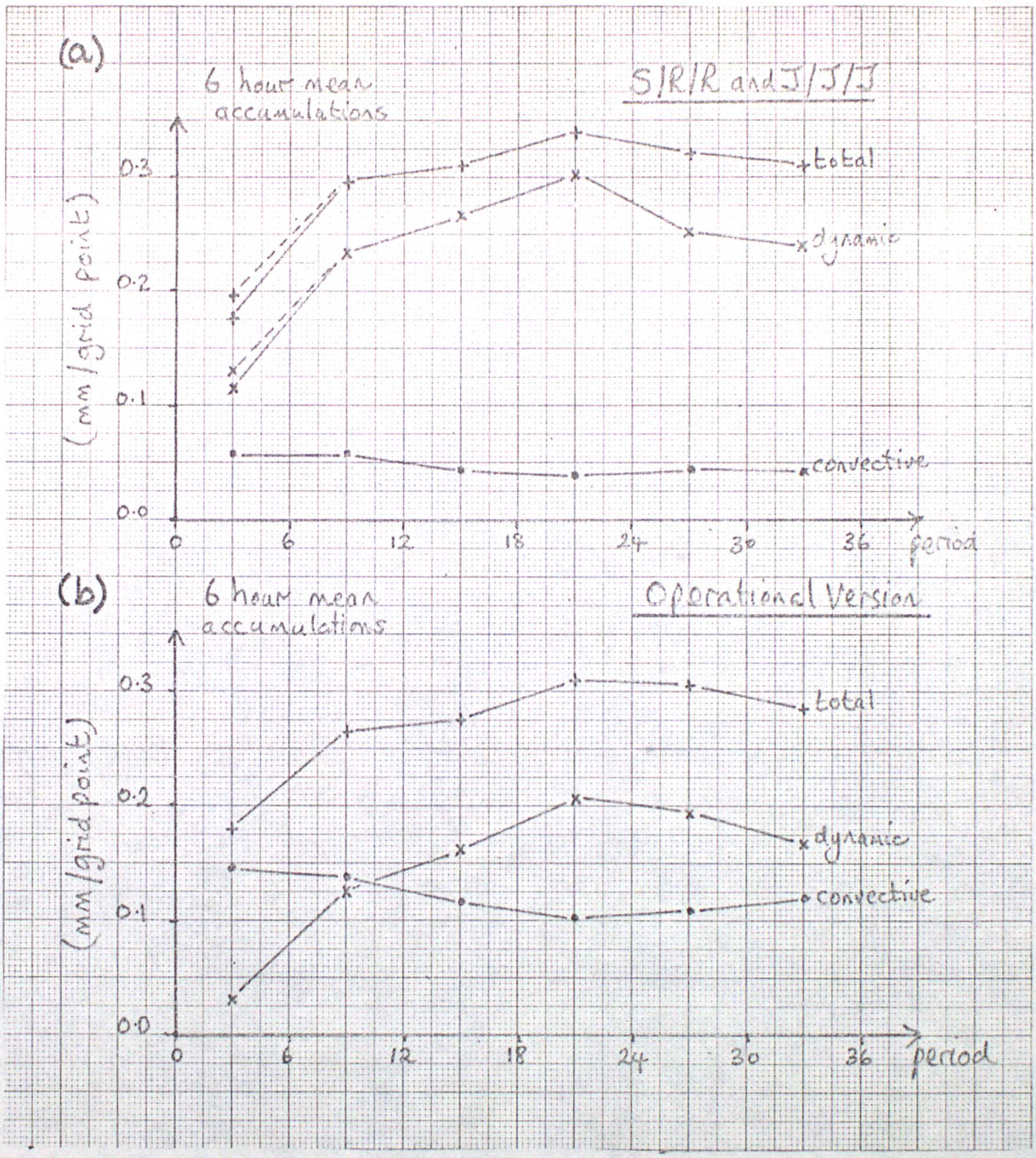

Figure 11

6 hour rainfall accumulations for (a) the J/J/J and S/R/R schemes, and (b) the operational scheme

FORECAST SURFACE PRESSURE AND PRECIPITATION

36HOUR FORECAST.DATA TIME=0Z 30/6/77.VERIFICATION TIME=12Z 1/7/77

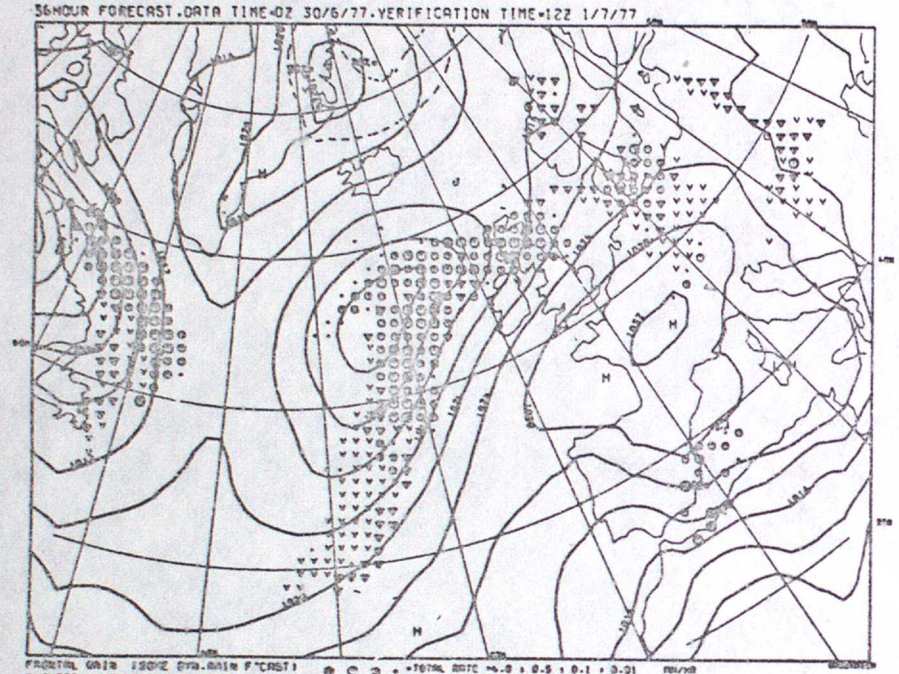

RATE OF DYNAMIC RAIN ISOPLETHS AT 0.5 MM/HR

36HOUR FORECAST.DATA TIME=0Z 30/6/77.VERIFICATION TIME=12Z 1/7/77

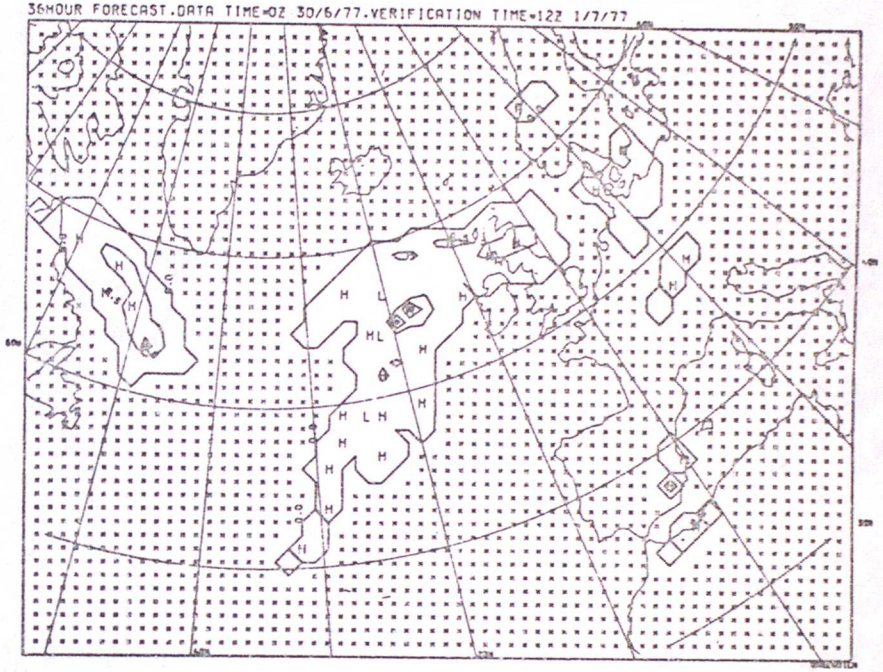

TOTAL RATE OF RAIN 0.5 MM ISOHYET INTERVAL

36HOUR FORECAST.DATA TIME=0Z 30/6/77.VERIFICATION TIME=12Z 1/7/77

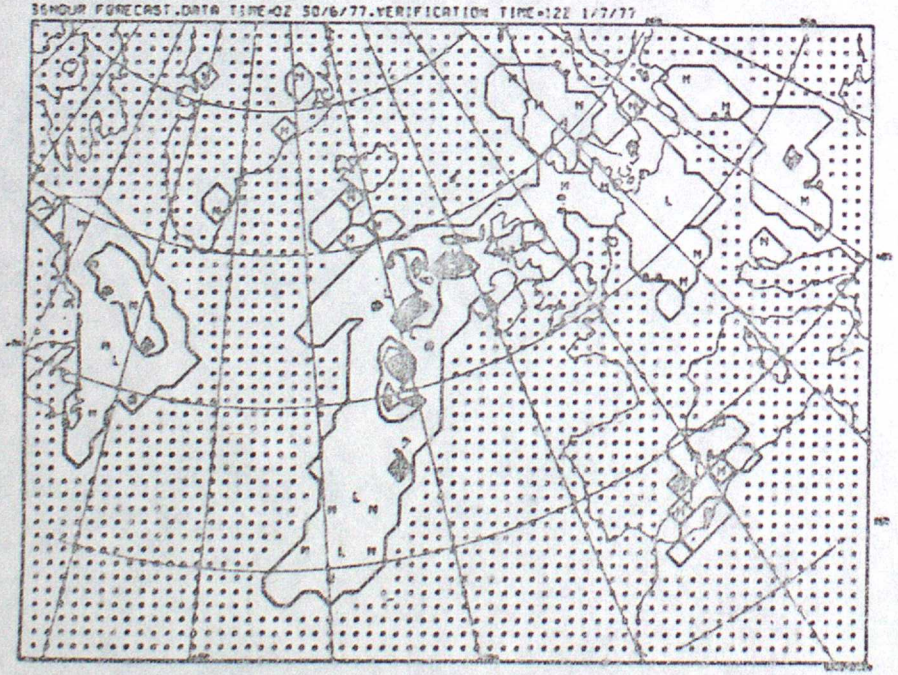

RATE OF CONVECTIVE RAIN ISOPLETH AT 0.25 MM/HR

36HOUR FORECAST.DATA TIME=0Z 30/6/77.VERIFICATION TIME=12Z 1/7/77

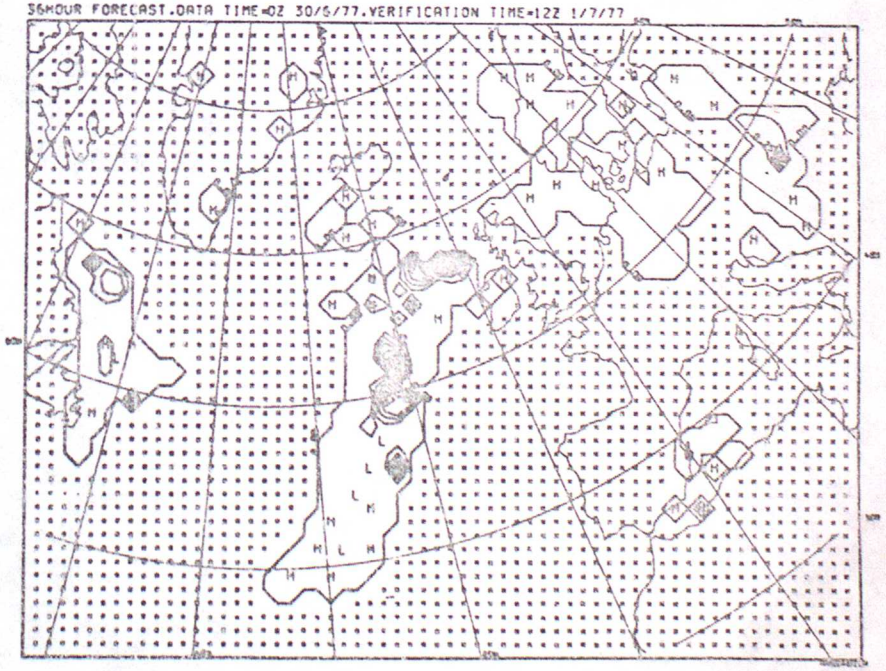

Figure 12- 36 hour forecast using the operational condensation scheme

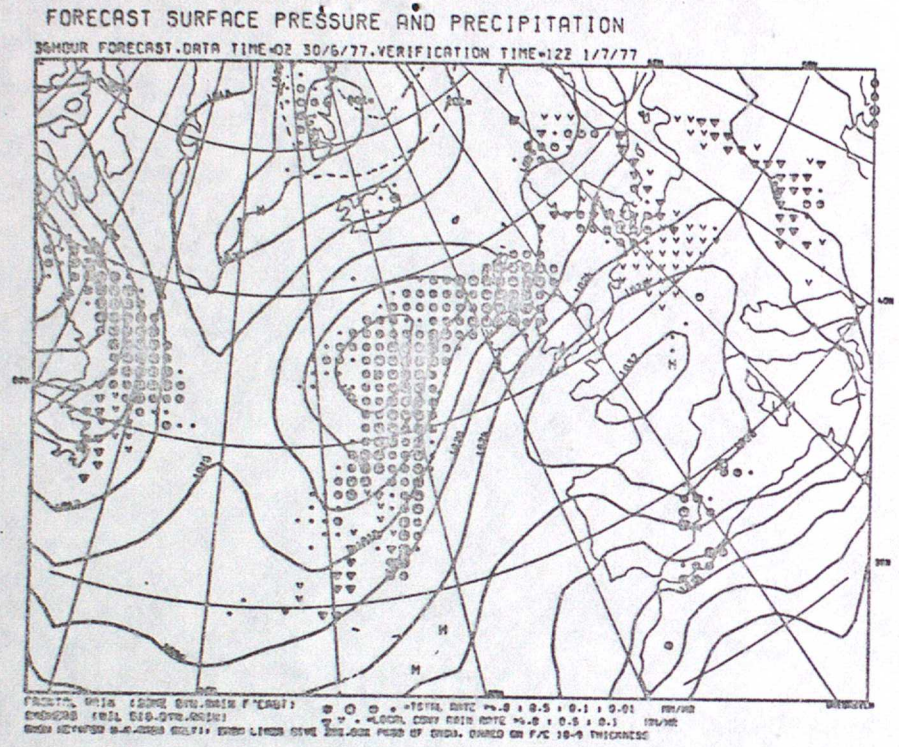

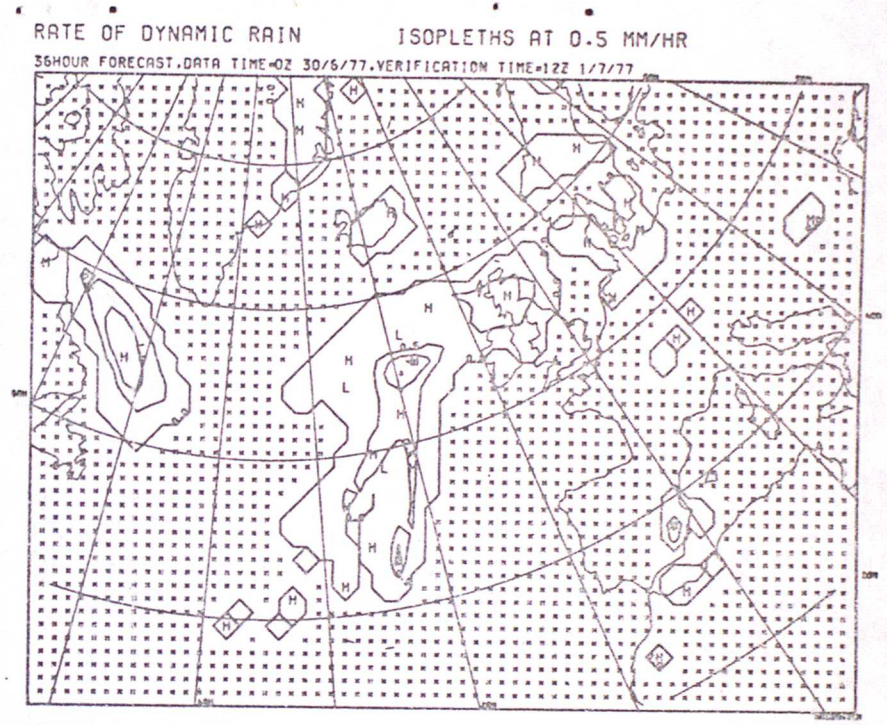

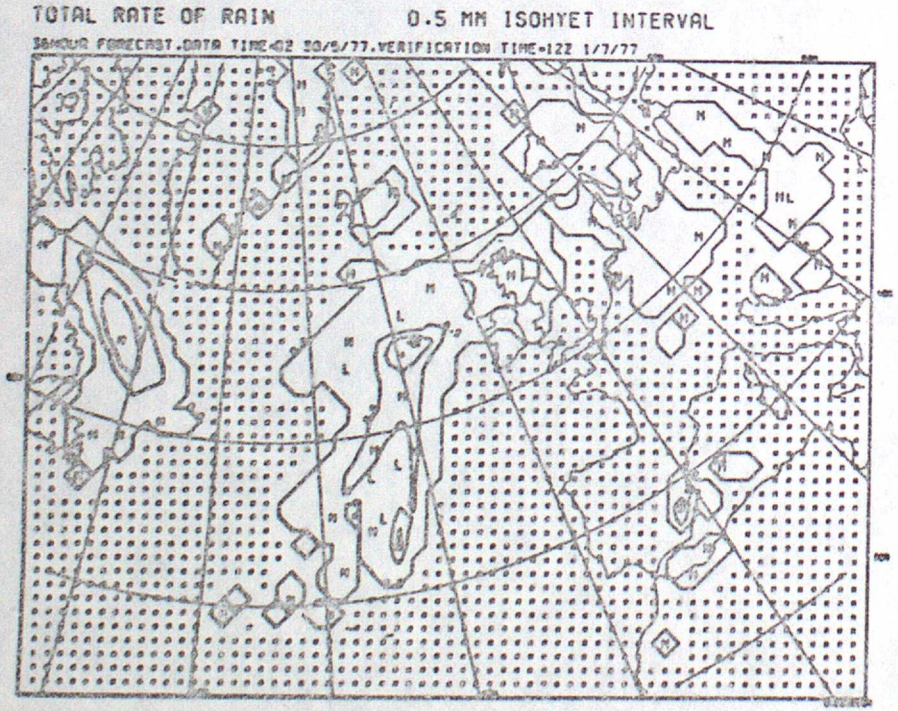

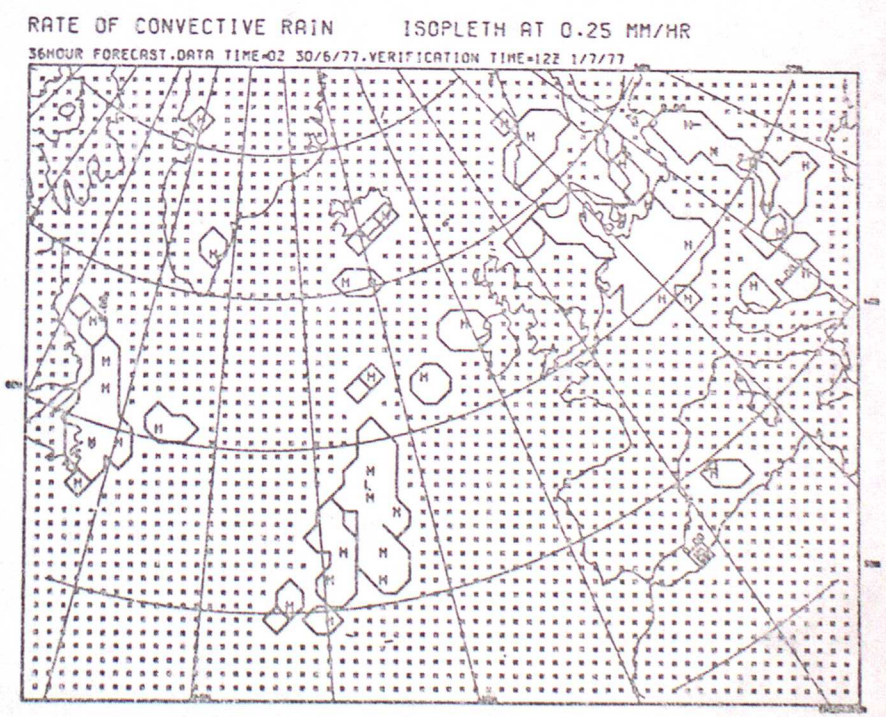

Figure 13- 36 hour forecast using the S/R/R condensation scheme

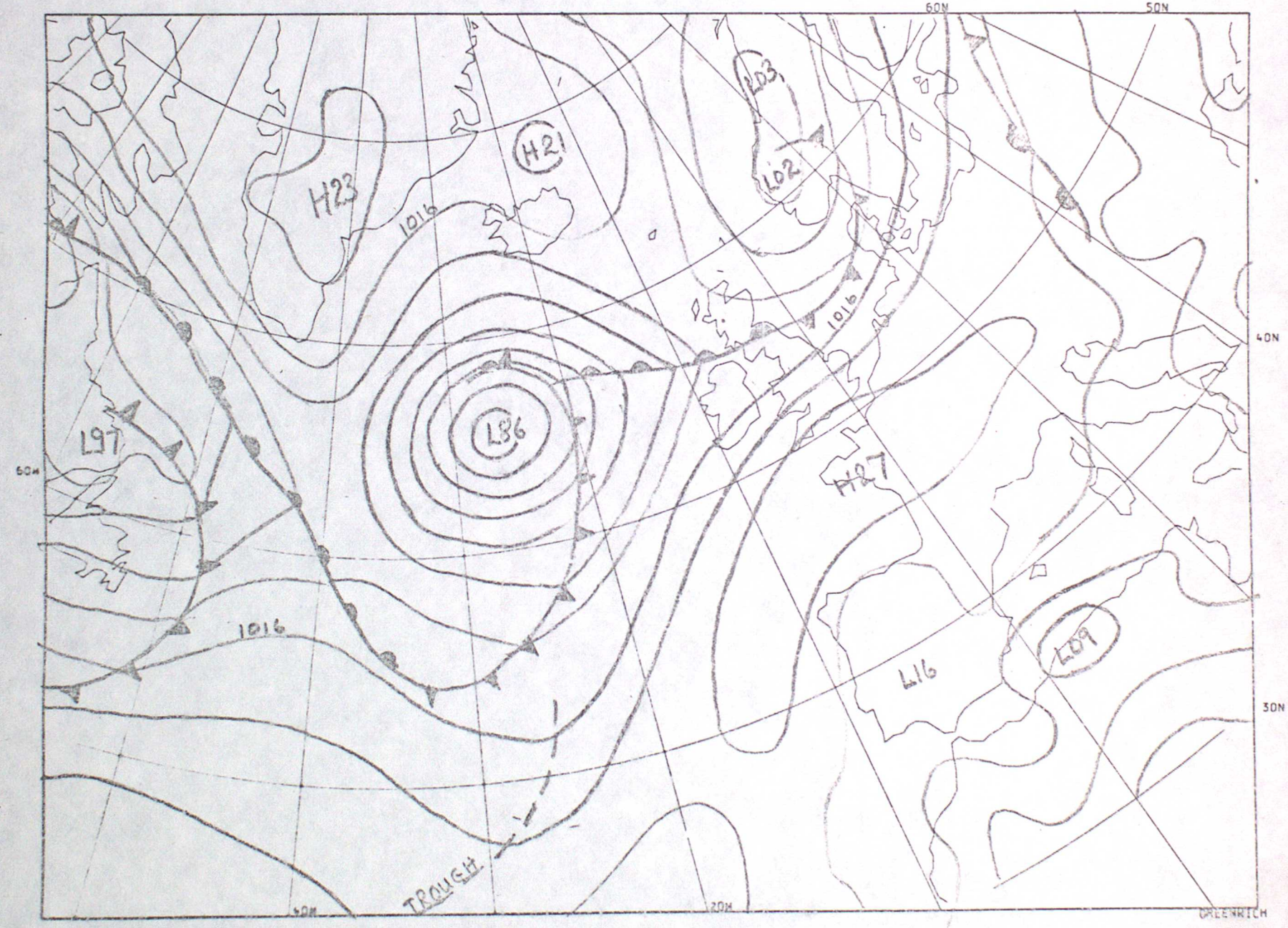

Figure 14 - surface analysis at 12Z 1/7/77

XXX - frontal cloud /// - cloudy

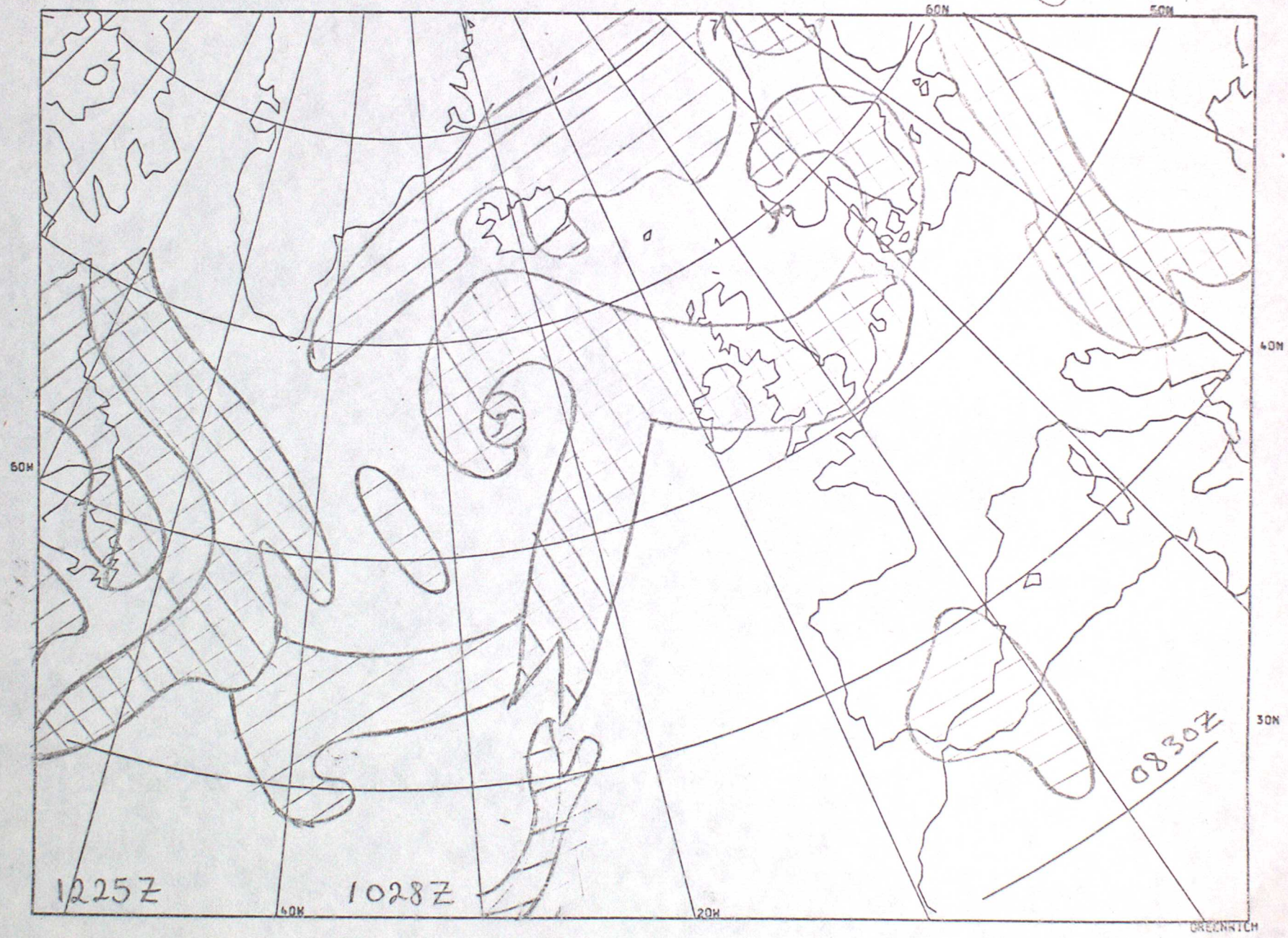

Figure 15 - nephanalysis at about - 12Z - 1/7/77

Figure 16

36 hour forecast of fractional cloud cover using S/R/R (V.T. 12Z 1/7/77)

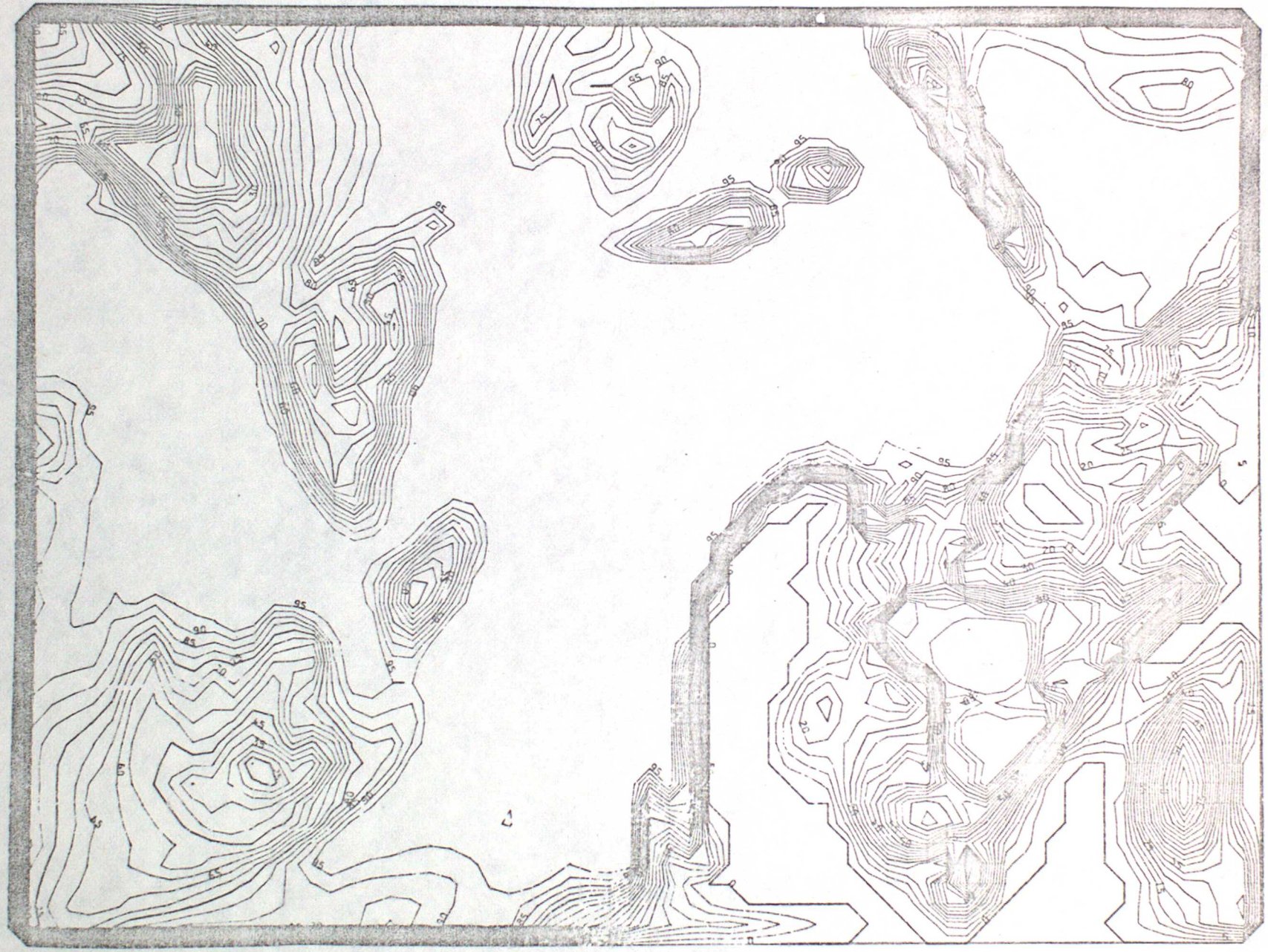

Figure 17
36 hour forecast of fractional cloud cover using the Burridge and Gadd formulation (V.T. 12Z 1/7/77)

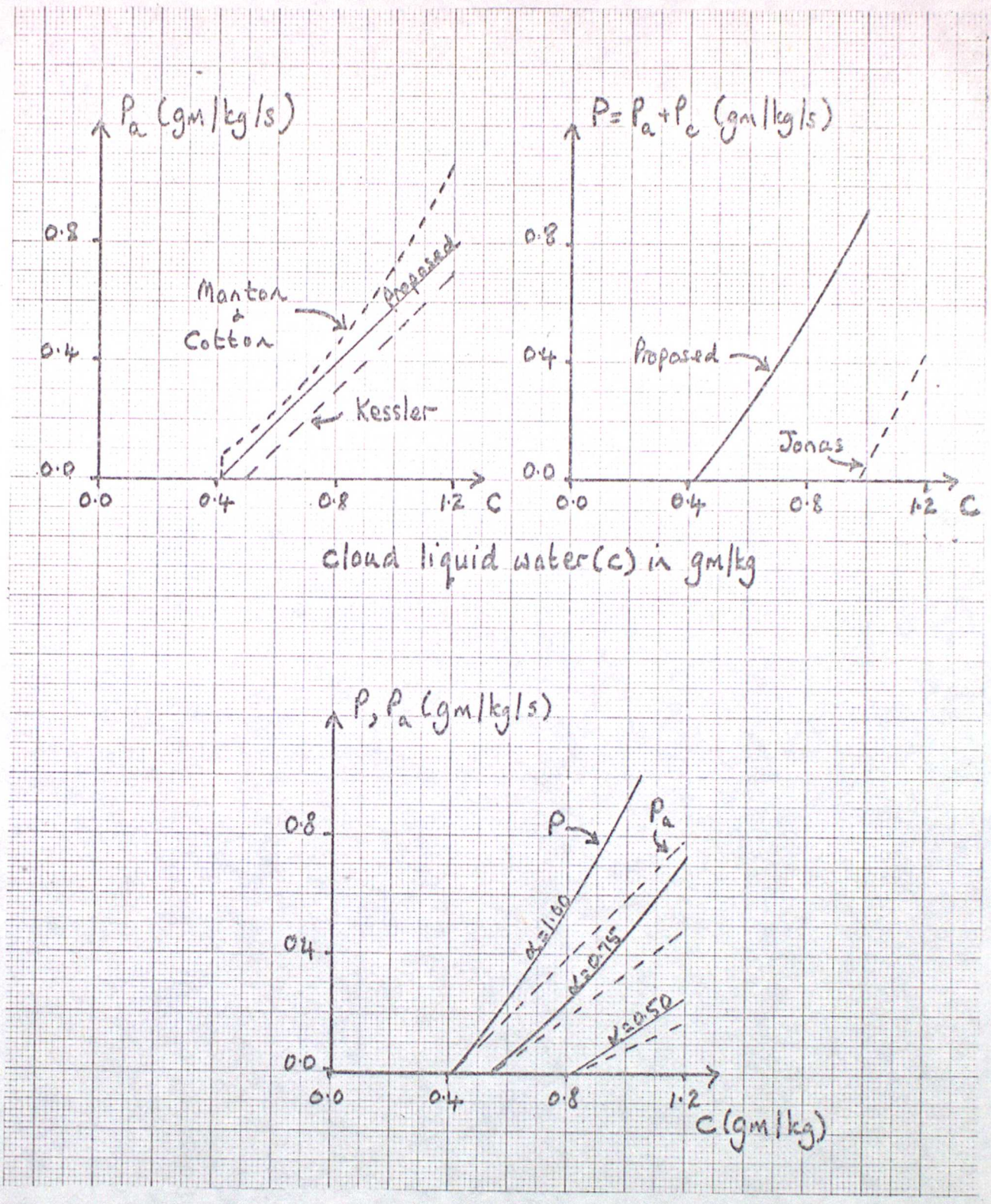

Figure A1

Autoconversion rate (P_a) and total conversion rate ($P = P_a + P_c$) for various formulations

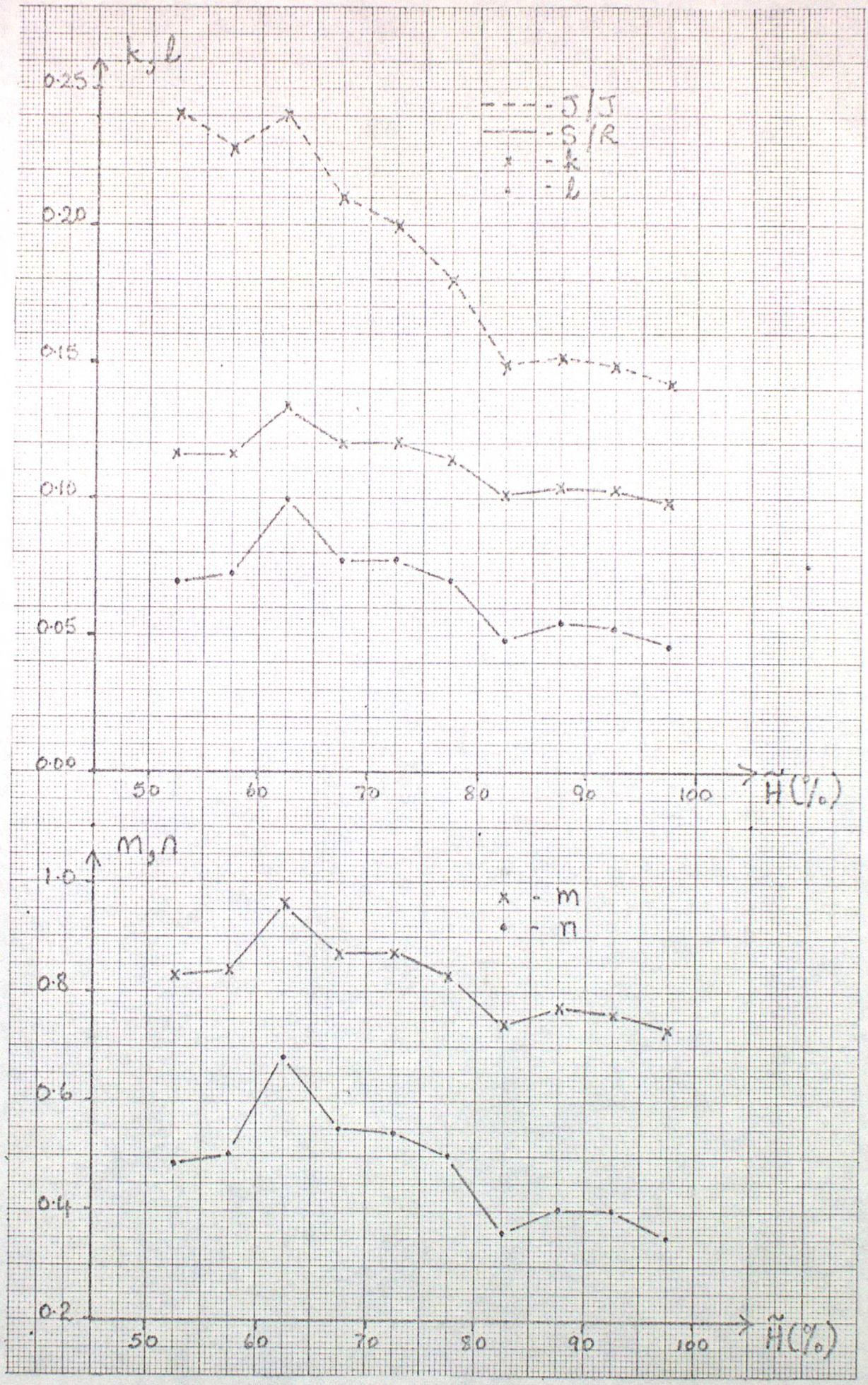

Figure A2

Estimates of autoconversion thresholds using 850mb humidity observations

Table A1

Relative Humidity ($\tilde{H}$)	$\mathfrak{H} = P/P_w$
0.525	21.00
0.575	16.67
0.625	22.33
0.675	11.57
0.725	8.96
0.775	6.26
0.825	3.44
0.875	3.17
0.925	2.56
0.975	1.86